

國立交通大學

奈米科技研究所

碩士論文

利用奈米生物科技研究自組裝蛋白質

Application of bionanotechnology to study self-assembled proteins

研究生：林志杰

學 號：9452512

指導教授：黃國華 副教授

中華民國九十六年七月

利用奈米生物科技研究自組裝蛋白質

學生：林志杰

指導教授：黃國華 副教授

國立交通大學奈米科技研究所 碩士班

中文摘要

第一部份：

科學家對蜘蛛絲有極大的興趣，因其具有相對人造絲更良好的機械特性。本實驗取出人面蜘蛛絲主絲囊的蜘蛛絲蛋白質，並研究出可穩定保存蜘蛛絲蛋白質的保存液。更進一步利用蜘蛛絲蛋白質混合有機溶液來達成自組裝成絲狀及網狀的結構。

第二部份：

我們利用高效能液相層析儀 [high-performance liquid chromatography (HPLC)] 配合膠體過濾法來純化並分析核糖體。粗粹取物利用大腸桿菌 XL1-Blue 經由超高速離心來得到核糖體。大腸桿菌粗粹取物 70S 核糖體於高效能液相層析儀分析出單一峰值，核糖體是由粗粹取物經高速離心純化而得到。而高效能液相層析儀純化之核糖體之雜質較高速離心純化得到核糖體之雜質為少。經由高效能液相層析儀純化之核糖體吸光值比值 (260nm/280nm) 可達 2.31，而高速離心純化得到核糖體之只有 1.92。當環境溫度為 42°C 時，經由高效能液相層析儀純化之核糖體較高速離心純化得到核糖體來的穩定。高效能液相層析儀也偵測 50S 和 30S 的結合，也經由穿透式電子顯微鏡證實，而這些變化應為缺少鎂離子所造成。目前的研究提供了一個核糖體純化和結構變化分析的平台。

Application of bionanotechnology to study self-assembled proteins

Student: Chie-Chieh Lin

Advisors: Dr. Guewha Steven Huang

Institute of Nanotechnology National Chiao Tung University

Abstract

Part I:

Spider silks have extraordinary mechanical properties. Even man-made fibers cannot achieve them. In this study we collected major silk gland from *Nephila pilipes*. Found out the stable buffer to storage spidroin. Application of spidroin with organic solvents to induce self-assembled silk-like and net-like structures.

Part II:

We established a high-performance liquid chromatographic (HPLC) system with gel filtration column for the purification and analysis of ribosomes. Crude extract was prepared from *Escherichia coli* XL1-Blue and went through ultra-centrifugal procedure to obtain ribosomes. 70S ribosome appeared as single peak in the HPLC chromatogram analyzing *E. coli* crude extract. Ribosomes were purified from crude extract and from ultra-centrifugation prep. HPLC-purified ribosomes contained fewer impurities than ribosomes prepared from ultra-centrifugal procedure. OD 260nm/280nm ratios of HPLC-purified ribosomes achieved 2.31, while the best ultra-centrifugal prep was only 1.92. When incubated at 42 °C, HPLC-purified ribosomes presented improved stability compared to conventionally purified ribosomes. This HPLC system was also capable of detecting conformational change of ribosomes. In the absence of magnesium ion, HPLC detected aggregation of 50S and 30S subunits which were confirmed by electron microscopy. A higher order of conformational reorganization might have occurred in the absence of magnesium ions. The current study provided an alternative platform for the purification and conformational analysis of ribosomes.

誌 謝

經過大學四年的努力，進了這令我嚮往的國立交通大學，原來就讀材料工程系，轉而進入了一個熱門的”奈米”研究所，讓我感到非常的興奮。進入奈米所以後，非常幸運的跟隨一位研究奈米生物方面的老師 黃國華 副教授兼所長，讓我學習到除了以往的材料相關的知識外，又添加了生物方面的專長，雖然不一定學得很專精，但在老師教導下，慢慢地更進一步對生物方面瞭解了，也因為老師的研究方向，讓我的研究添加了一些未知的領域，使得我對生物方面的研究越來越感興趣。現在的人，最需要的就是”跨領域”的學習，專一的研究固然重要，但是當加入了另一個新的領域時，將引領學生擁有更多方向的探索，這是很可貴的，而本實驗室就擁有這種益處。兩年的時間，轉眼間就到了，黃國華 實驗室讓我學習了很多，不僅研究方面有老師的專業指導；生活上，老師、師母 洪孟燕 小姐、洪耀欽 醫師，都給予了相當的關懷及照顧，畢竟這不是所有實驗室能教授的知識、經驗。兩年內的時間，需要感謝的人太多，首先感謝老師在研究上的細心指導，不管多晚也歡迎學生去討論，也感謝用心栽培我的師母，辛辛苦苦為了我的研究去山上抓蜘蛛、教導我學習應該有的態度、讓我學會管理帳務，也感謝碩一時帶我的耀楠學長、凱明學長，以及同屆的實驗伙伴：嘉偉、永昌、禮閣，讓我在這兩年內，不僅有了研究上的伙伴，也添

加了生活上的樂趣。即將離開實驗室，心中有萬般的不捨，願我們實驗室能越來越好，祝福實驗一切順利，也祝福從這裡畢業的學生能帶著兩年內的豐富經歷，並以本實驗室為榮，邁開腳步往下一個新的人生階段前進。



Contents I

Chapter 1 : Introduction.....	I-1
1.1 : Special characteristic of spider silk	I-1
1.2 : Spider silk types and their proteins.....	I-4
1.3 : Study for forming spider silk.....	I-15
1.4 : Application of protein as self-assembled motif to produce nanostructure	I-21
Chapter 2 : Experiment Design, Materials and Methods	I-27
2.1 : Experiment Design	I-27
2.2 : Chemicals	I-28
2.2.1 : Spider species.....	I-28
2.2.2 : Stable buffer for Spidroin	I-28
2.2.3 : SDS-PAGE chemicals.....	I-29
2.2.4 : High performance liquid chromatography.....	I-31
2.2.5 : Electron microscopy fixation and dehydration chemicals	I-31
2.3 : Instruments	I-31
2.3.1 : SDS-PAGE electrophoresis	I-31
2.3.2 : High-performance liquid chromatography.....	I-32
2.3.3 : Scanning Electron Microscopy	I-41
2.4 : Experiments	I-42
2.4.1 : Find the stable condition for Spidroin from major gland.....	I-42
2.4.2 : Analysis of Spidroin by SDS-PAGE	I-43
2.4.3 : Analysis of Spidroin by High performance liquid chromatography.....	I-43
2.4.4 : Preparation of gold nanoparticles	I-44
2.4.5 : Self-assemble of spidroin to form protein nanostructure.....	I-44
2.4.6 : Self-assembled protein nanostructures with gold nanoparticles.....	I-45
2.4.7 : Organic solvents induced protein structure.....	I-45
2.4.8 : Scanning electron microscopy of Self-assembled protein nanostructure	I-46

Chapter 3 : Results and Discussion	I-47
3.1 : Stable condition for spidroin from major gland.....	I-47
3.2 : SDS-PAGE analysis of spidroin	I-48
3.3 : High performance liquid chromatography analysis of spidroin	I-49
3.4 : Self-assembled protein nanostructures	I-50
3.5 : Self-assembled protein nanostructures combined with gold nanoparticles	I-51
3.6 : Organic solvents induced protein structures.....	I-52
3.6.1 : Methanol treatment with spidroin	I-54
3.6.2 : Ethanol treatment with spidroin	I-55
3.6.3 : Isopropyl alcohol treatment with spidroin	I-56
3.7 : Summary.....	I-57
Chapter 4 : Conclusion	I-57
Chapter 5 : Future perspective.....	I-58
Chapter 6 : References.....	I-58



Table Contents I

Table 1: Spider silks and their uses (left table), comparisons of mechanical properties of spider silk (right table).....	I-3
Table 2: Hypothesized relationships between molecular structure, mechanical performance, and ecological use of silks spun by <i>Arigiope crgentata</i>	I-3
Table 3: Tensile mechanical properties of spider silks and other materials.	I-3

Figure Contents I

Fig 1: The silk glands and threads of <i>Araneus diadematus</i>	I-4
Fig 2: Models for the molecular architecture of <i>Araneus diadematus</i> major ampullate gland silk.(from [6])	I-6
Fig 3: Hierarchical structure of spider dragline silk <i>N. pilipes</i>	I-6
Fig 4: SEM image of a fiber of tubuliform silk.....	I-12
Fig 5: Spinning pathway of spider.....	I-18
Fig 6: Drawing of dissected major ampullate gland and associated structures taken from a light micrograph.	I-18
Fig 7: The proposed stages in lamellar liquid crystalline assembly of the nano fibrils of the major ampullate (dragline) silk thread in orb web spiders (see text) showing.	I-19
Fig 8: A spider's dragline spinneret.	I-20
Fig 9: TEM image of unstained film prepared from 0.001% PEP-PI2200 copolymer in 2:1 v/v $\text{CHCl}_3/\text{HOCH}_2\text{CH}_2\text{Cl}$	I-22
Fig 10: TEM images of Au nanocrystals on the sequenced histidine-rich peptide nanotubes.	I-22
Fig 11: SFM image of the peptide nano-doughnuts.	I-23
Fig 12: Model for flagella nanotube self-assemble and disassemble.	I-23
Fig 13: Model for fabricating a coaxial nanowire.....	I-24
Fig 14: Ordered organization of the nanoparticles on the nanotubes.	I-24
Fig 15: Tapping mode AFM topological plots of $(\text{Ala})_4$ (left image) and $(\text{Ala})_6$ (right image) spin-coated film on a silicon wafer. (from [44]).....	I-25
Fig 16: SEM images of spider silk as scaffold for the one-step synthesis and assembly of gold nanoparticles.....	I-25
Fig 17: Electron micrographs of negatively stained (2% uranyl acetate) fibrils.	I-26
Fig 18: The photograph is a mature female <i>Nephila pilipes</i>	I-28
Fig 19: The abdominal part of the spider.....	I-42
Fig 20: The major ampullate glands of spider.	I-42
Fig 21: The phase diagram of spidroin.	I-47
Fig 22: SDS-PAGE electrophoresis of spidroin.	I-48
Fig 23: Gel-filtration of spidroin.	I-49
Fig 24: SEM images of self-assemble protein nano structures.	I-50
Fig 25: SEM images of self-assemble protein nano structures with 37nm gold nanoparticles.	I-51
Fig 26: SEM images of methanol induced protein structures.	I-54
Fig 27: SEM images of ethanol induced protein structures.	I-55
Fig 28: SEM images of isopropyl alcohol induced protein structures.	I-56

Contents II

Chapter 1 : Introduction.....	II-1
Chapter 2 : Paper Review	II-3
2.1 : Introduction of Prokaryotic Ribosome	II-3
2.2 : Conventional Ultra-Centrifugal Purification of Prokaryotic Ribosome	II-3
2.3 : Motivation.....	II-6
Chapter 3 : Materials and Methods	II-7
3.1 : Chemicals	II-7
3.1.1 : Buffer solutions for purification of ribosome	II-7
3.1.2 : Solutions for Cryo-Transmission Microscopy	II-8
3.2 : Instruments	II-9
3.2.1 : Autoclave	II-9
3.2.2 : French pressure cell press	II-10
3.2.3 : UV-Visible Spectrophotometer.....	II-11
3.2.4 : High-performance liquid chromatography.....	II-11
3.2.5 : Cryo-Transmission Electron Microscopy	II-12
3.3 : Experiments	II-13
3.3.1 : Purification of Bacterial Ribosome by Ultracentrifugation	II-13
3.3.2 : Analysis of Ribosome by HPLC-gel Filtration.....	II-14
3.3.3 : Further Purification of Bacterial Ribosome by HPLC-gel Filtration.....	II-14
3.3.4 : Cryo-Transmission Electron Microscopy	II-15
Chapter 4 : Results and Discussion	II-16
4.1 : Analysis of Ribosome by HPLC-gel filtration	II-16
4.2 : HPLC further Purification and Analysis for Ribosome.....	II-20
4.3 : The Absence of Magnesium Promoted Aggregation of Ribosomes	II-26
Chapter 5 : Conclusion	II-28
Chapter 6 : References.....	II-29

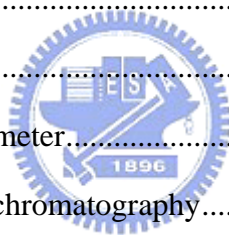


Figure Contents II


Fig 1: The growth curve of <i>E. coli</i> XL1-Blue.	II-17
Fig 2: HPLC gel-filtration of each purification process.	II-18
Fig 3: HPLC gel-filtration of each purification process with 10mM MgCl ₂	II-19
Fig 4: HPLC-gel filtration analysis of prokaryotic ribosomes.	II-21
Fig 5: Cryo-Electron microscopic image indicated intact 70S ribosome conformation.	II-22
Fig 6: Cryo-EM images of ribosomal fractions collected from HPLC-purification.	II-23
Fig 7: OD ₂₆₀ /OD ₂₈₀ of HPLC-purified ribosomes compared to ultra-centrifugation-purified prep.	II-24
Fig 8: Thermal stability test on HPLC-purified and partially purified ribosomes.	II-25
Fig 9: HPLC analysis of purified ribosomes at various concentrations of magnesium ions.	II-27



Chapter 1 : Introduction

Spider silk has been extensively studied for its outstanding mechanical properties. There are many research focused on its silk, protein, and applying silk-like peptide to assemble protein structure. No previous studies mentioned directly apply spidroin to assemble protein nano structure[1, 2]. In our research, we found the stable solution to storage the spidroin, and analyzed these spidroin. We also used some organic solvents to denature the spidroin, then formed special protein nanostructure. We hope to application of these protein nanostructures to design composite materials. We tried to combine inorganic material-nano gold particle to our protein structure. Results show the scanning electron microscopy of these self-assembled protein structure.

1.1 : Special characteristic of spider silk



Silks have attracted the interest of scientists of various disciplines for a long time. Initially, this interest was inspired by the importance of silkworm silk in the manufacture of high-quality textiles. Attempts to make synthetic fibers mimicking the basic structural motifs and properties of native silk resulted in the invention of high-performance polyamide materials such as Nylon and Kevlar, which have had an important impact extending beyond the textile industry. Although many insects and spiders are known to produce silks, until today the cocoon silk of the silkworm, *Bombyx mori*, remains the only native silk fiber that can be cultivated and commercialized. Since advances in biotechnology now have opened new pathways for the controlled large-scale production of proteins with predetermined amino acid sequences, materials scientists, polymer chemists, and bioengineers have become increasingly interested also in other kinds of silks and silk-producing organisms that so far have escaped cultivation. In contrast to silkworms, spiders are remarkable in their ability to spin a variety of different silks, each of which has been optimized with respect to its specific

biological function by nature. Thus spiders can teach us important lessons about structure function relationships of biomaterials based on proteins [3].

Silk is of vital importance for a spider. Indeed, orb-weaving spiders can produce up to seven types of silks, each with a specific function and unique properties. The major ampullate (MA) silk that forms most of the safety line (dragline) and radial fibers of the web has received the most attention. The dragline exhibits great tensile strength combined with good extensibility thus giving it a toughness greater than most man-made fibers, including steel. To achieve those remarkable properties, spiders have evolved well-designed elastomeric silk proteins, as well as complex and unique spinning glands.

Spider major ampullate (dragline) silk is of practical interest because of its excellent mechanical properties. Spiders make their webs and perform a wide range of tasks with up to seven different types of silk fiber in seven highly specialized glands. Spiders have the ability to produce a wide range of different silks for a variety of purposes including ballooning, egg protection, or prey capture. The major ampullate silk makes structural and dragline silk, minor ampullate is for auxiliary spiral silk, piriforme is responsible for attachment cement, aciniforme is for wrapping silk and packing silk, cylindrical is cocoon silk, aggregate is for sticky silk glue, flagelliforme is thread for sticky silk (see Fig. 1 and Table 1). Although there are seven different types of silk, dragline silk fiber which is the product of the major ampullate gland, has been the most extensively investigated silk fiber because of an interesting combination of high tensile strength, extensibility, and an energy-dissipative viscoelastic response. Table 1 and 3 lists mechanical properties of several spider silks from *N. clavipes* compared with some natural and manmade materials. Spider-silk fibers are nearly as strong as several of the current synthetic fibers and can outperform them in many applications in which total energy absorption is important. Our research emphasize on the spider ampullate silk protein.

Silk	Use	Spinneret	Material	Strength (N m ⁻²)	Elasticity (%)	Energy to break (J kg ⁻¹)
Major ampullate dragline	Web frame and radii	Anterior	Dragline silk (major ampullate)	4 × 10 ⁹	35	1 × 10 ⁵
Minor ampullate	Web reinforcement	Medial	Flagelliform silk	1 × 10 ⁹	>200	1 × 10 ⁵
Flagelliform	Core fibers of adhesive spiral	Posterior	Minor ampullate	1 × 10 ⁹	5	3 × 10 ⁴
Aggregate	Adhesive silk of spiral	Anterior and posterior	Kevlar	4 × 10 ⁹	5	3 × 10 ⁴
Cylindrical	Cocoon	Posterior	Rubber	1 × 10 ⁶	600	8 × 10 ⁴
Aciniform	Swathing and inner egg sack	Anterior	Tendon	1 × 10 ⁹	5	5 × 10 ³
Pyriform	Attachment disk and joining fibers	Anterior	Nylon, type 6	7 × 10 ⁷	200	6 × 10 ⁴

Table 1: Spider silks and their uses (left table), comparisons of mechanical properties of spider silk (right table). (from [4])

Silk	Molecular elements	Mechanical performance	Ecological function
Major ampullate	Composition: GA and poly(A) motifs, short repeats of GPGX _n motifs ^{1,2} 2 ^o structure: β -sheet crystals oriented along fiber axis embedded in amorphous matrix ^{3,4}	High tensile strength, low extensibility, high loss tangent, exhibits super contraction when wetted, higher hysteresis	Draglines, primary dry structural elements of most capture webs
Tubuliform	Composition: A and S rich, long and complex repeats lacking in subrepeat motifs ^{5,6} 2 ^o structure: β -sheets twist parallel to fiber orientation embedded in amorphous matrix ^{7,8,9}	High modulus, low strength, very little stiffening after fiber yield, consistently low storage modulus, loss tangent is relatively constant after fiber yield, thick diameter	Inner flocculent silk of egg sacs
Minor ampullate	Composition: GA motifs lack poly(A) motifs ¹ 2 ^o structure: β -sheet crystals oriented along fiber axis embedded in amorphous matrix ⁹	High modulus and extensibility, moderate tensile strength and toughness	Temporary spiral of orb, sometimes added to draglines
Aciniform	Composition: G, A and S rich, long, complex repeats lacking in subrepeat motifs ¹⁰ 2 ^o structure: uncharacterized	High modulus, extensibility and toughness, high storage modulus, multi-strand sheet of fine fibers	Prey wrapping, stabilimentum web decorations, outer layer of egg sacs
Capture spiral	Composition: core fiber (flagelliform silk gland) coated with glycoprotein glue, core fiber has long repeats of GPGX _n motifs ¹ 2 ^o structure: lacks β -sheet, subrepeats fold into molecular 'nanosprings', plasticized fiber ^{12,13,14,15}	Extremely extensible and resilient, highly compliant, glue-coated wet fiber	Sticky spiral of cribellate orb webs

Amino acids are indicated by one-letter abbreviations: A, alanine; G, glycine; P, proline; S, serine; X, glycine or other amino acid. ¹Gatesy et al., 2001), ²Xu and Lewis, 1990), ³(Parkhe et al., 1997), ⁴Thiel et al., 1997), ⁵(Garb and Hayashi, 2005), ⁶(Tian and Lewis, 2005), ⁷(Barghout et al., 2001), ⁸(Barghout et al., 1999), ⁹(Dicko et al., 2004), ¹⁰(Hayashi et al., 2004), ¹¹(Hayashi and Lewis, 2000), ¹²(Gosline et al., 1984), ¹³(Hayashi and Lewis, 1998), ¹⁴(Hayashi and Lewis, 2001), ¹⁵(Vollrath and Edmonds, 1989).

Table 2: Hypothesized relationships between molecular structure, mechanical performance, and ecological use of silks spun by *Arigiope crgentata*.

(from [5])

Material	Stiffness, E_{init} (GPa)	Strength, σ_{max} (GPa)	Extensibility, ϵ_{max}	Toughness (MJ m ⁻³)	Hysteresis (%)
<i>Araneus</i> MA silk	10	1.1	0.27	160	65
<i>Araneus</i> viscid silk	0.003	0.5	2.7	150	65
<i>Bombyx mori</i> cocoon silk	7	0.6	0.18	70	
Tendon collagen	1.5	0.15	0.12	7.5	7
Bone	20	0.16	0.03	4	
Wool, 100 % RH	0.5	0.2	0.5	60	
Elastin	0.001	0.002	1.5	2	10
Resilin	0.002	0.003	1.9	4	6
Synthetic rubber	0.001	0.05	8.5	100	
Nylon fibre	5	0.95	0.18	80	
Kevlar 49 fibre	130	3.6	0.027	50	
Carbon fibre	300	4	0.013	25	
High-tensile steel	200	1.5	0.008	6	

The data for *Araneus* silks are from Denny (1976) and our laboratory. Other data have been taken from Wainwright et al. (1982), Gordon (1978, 1988) and Vincent (1982), without specific references because they are intended to indicate the relative magnitude rather than exact values.

MA silk, silk from the major ampullate gland; RH, relative humidity.

Table 3: Tensile mechanical properties of spider silks and other materials.

(from [6])

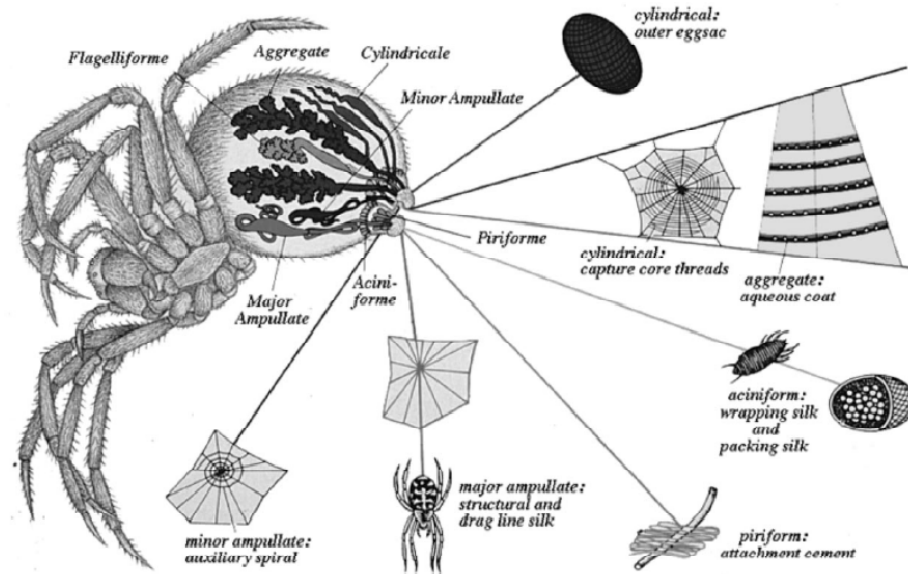


Fig 1: The silk glands and threads of *Araneus diadematus*.

The glands are called by their Latin names, which are again referred when associated with the type of silk they produce (reprinted from Wynne, 1992). (from [2])

1.2 : Spider silk types and their proteins

Spiders are capable of producing up to seven types of silk. Each silk has a specific function, with the silk of the major ampullate glands being the most prominent.

Orb web spiders are capable of producing up to six different types of silk, as well as a glue substance, that have various biological functions (Fig. 1). The different silk types are protein-based polymers that are members of the spider silk protein superfamily and display restricted expression in seven morphologically distinct silk glands. These distinct abdominal glands are thought to have evolved from a single type of gland, and have subsequently diverged in their anatomy, luminal contents and morphology. Based upon the differential amino acid compositions of the luminal contents, the silk proteins within each gland are proposed to be assembled to create specific fibers with particular functions. To date, most research has focused on the major ampullate gland, which manufactures dragline silk constituents. Dragline silk is well known for its combination of high tensile strength and elasticity, which leads to a fiber with extraordinary toughness. Spiders use dragline silk to

create web anchors, as well as safety-lines for survival (Fig. 1). The minor ampullate gland, which shares morphological similarity to the major ampullate, synthesizes web radii filaments and temporary capture silk. Other abdominal glands produce silk types that participate in the direct capture of prey; these tissues include the flagelliform, aggregate and aciniform glands (Fig. 1).

Capture silk, also known as viscid silk, is a composite silk that contains material derived from the flagelliform and aggregate glands. Flagelliform gland silk is extremely extensible and forms the capture spiral of an orb web; this elasticity has been proposed to facilitate prey capture, enabling webs to arrest the motion of flying organisms without breaking. Aggregate glands have been postulated to manufacture spider glue proteins for silk fibers that coalesce to form sticky droplets, which interact with the capture spiral silk to influence the mechanical properties of the spiral filaments. The droplets have been shown to consist of a glycoprotein mixture, as well as a number of small molecules related to neurotransmitters.



Wrapping silk, which is used to entangle prey and build sperm webs as well as some constituents of egg case silk, is manufactured by the aciniform gland and has different molecular properties relative to viscid silk (Fig. 1). Tubuliform silk, also known as egg case silk, is produced from female tubuliform glands and provides protection for the encased eggs (Fig. 1). Egg cases must be tough enough to resist parasitic invasion and climate changes, and studies indicate that ancient female spiders constructed egg case sacs for protection of their developing offspring, whereas males used the egg case fibers to deposit sperm that could be transferred to the copulatory pedipalps. Perhaps the least studied gland, known as the pyriform gland, has been proposed to secrete materials that form attachment discs; these discs fasten threads of dragline silk to each other or to substrates.

Dragline silks

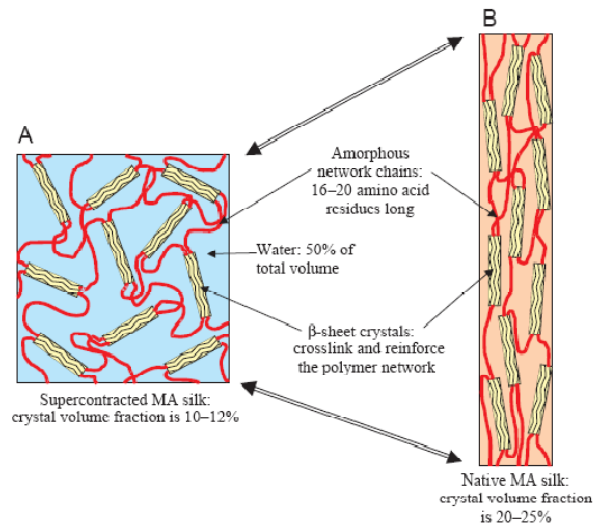


Fig 2: Models for the molecular architecture of *Araneus diadematus* major ampullate gland silk.(from [6])

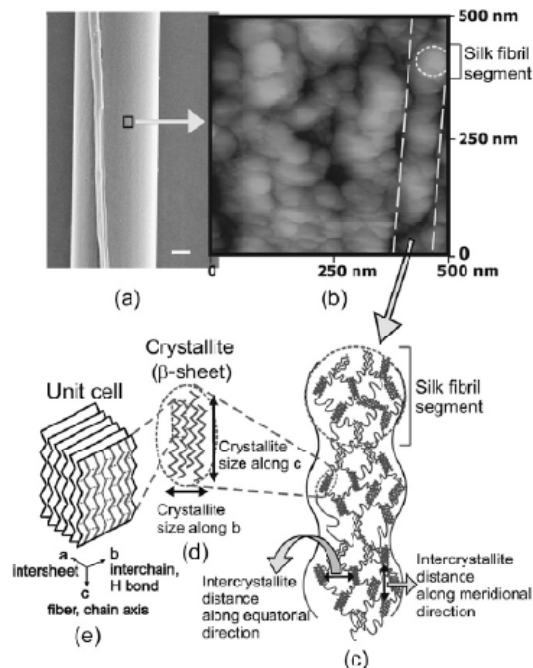


Fig 3: Hierarchical structure of spider dragline silk *N. pilipes*.

(a) SEM image of spider dragline silk. Scale bar, 1 μ m. (b) AFM image showing the silk fibril structure as the dashed lines indicate. Each silk fibril is composed of interconnected silk fibril segments as indicated by the dashed circle of size 40~80 nm. (c) Proposed model for the silk fibril structure: the silk fibril segment consists of several β -sheets connected by random coil or α -helix forming a protein polypeptide chain network. The mesh size of the network is the intercrystallite distance. (d) The crystallites in silk fibril have a β -sheet structure. The crystallite size and orientation can be determined by X-ray diffraction. (e) Unit cell of silk crystallite has an antiparallel β -sheet configuration. (Dashed lines indicate the hydrogen bonds between protein chains within one β -sheet.) (from [7])

All dragline silk core fibers have been shown to contain more than one protein, with molecular weights up to several hundred kilodaltons [8, 9]. Spidroin 1 and spidroin 2 are two of the dragline silk subunits that are produced in the major ampullate glands [9]. These proteins have been named major ampullate spidroin 1 and 2 (MaSp1 and MaSp2). MaSps have been shown to contain short peptide motifs that are repeated multiple times with various combinations to form repetitive structural modules, which range in size from 19 to 46 residues [4]. The repetitive regions of MaSp1 have been shown to be essentially proline free, whereas MaSp2 iterated sequences contain ~15% proline (Fig. 2). Partial cDNA clones that encode the two protein components have been isolated and characterized, largely from orb- and cob-weavers [1, 10]. Western blot studies indicate MaSp1 protein levels are higher in *Nephila clavipes* dragline silk, relative to MaSp2 [9]. In addition, structural studies of this dragline fiber using immunostaining are consistent with this finding, demonstrating that MaSp1 constitutes the bulk of the threads [11]. Collectively, these reports support the calculated amino acid composition of the fiber based upon proline content, which suggests the fiber contains 81% MaSp1 and 19% MaSp2 [12]. The question arises whether these percentages are universal in other dragline silks from other spider species. Recent evidence suggests that different spider species have markedly different ratios of MaSp1 and MaSp2 assembled into dragline silk relative to *N. clavipes*. For example, the orb weaver *Argiope aurantia* produces a dragline silk fiber that contains 41% MaSp1 and 59% MaSp2 [12]. In part, these differences may reflect the diet of the particular spider species, as dietary effects have been shown to affect the amino acid composition profiles of dragline silk [13]. Based upon the well-documented interspecies and intraspecies variations in the mechanical properties of dragline silks, it would seem plausible that changes in these spidroin ratios, along with the spinning conditions, could dictate the performance of the fibers [14]. Therefore, in the end, the composition of MaSp1 and MaSp2 assembled into the fiber is likely balanced by the pool of amino acid resources available to the spider, as well as the particular habitat of

the spider [15]. When resources and spinning conditions are ideal, a higher-performance fiber suited for the spider's needs is spun; however, when resources are limiting, the spider likely shifts the ratios of major ampullate spidroins to engineer a metabolically cheaper, lower-performance silk. In addition to the presence of internal repetitive modules within the primary sequences of MaSp1 and MaSp2, they both have been shown to contain nonrepetitive N and C termini [1]. C terminus length, as well as amino acid sequence, has been shown to be conserved across spiders of diverse phylogenetic origin for the Flag, MaSps and MiSps silk paralogues [16]. The strong conservation of the C-terminal region over several hundred million years implies an important structural role. Initially, two functions were proposed for the C-terminal region, which included (i) a role as a signal peptide and (ii) as a participant necessary for controlling the solubility of the spidroins in the highly concentrated spinning dope [17-19]. Although these functions are not mutually exclusive, recent studies have revealed that the major ampullate silks retain their C termini after extrusion. Because signal sequences are typically removed in the mature protein, their retention in the extruded fiber reduces the likelihood that they function as signal sequences. Evidence to support a role of the C termini in the conversion between the liquid to crystalline phase is beginning to gain scientific support. Localized regions of the nonrepetitive C termini have recently been demonstrated to modulate both the solubility and aggregation of the fibroins, with the conversion between these different physical states being highly dependent upon the environmental conditions [18].

One biological event that likely controls the natural spinning process is the hydrogen ion concentration. Certain residues within the C termini have been proposed as targets for ionization state changes, which might play an important role in initiating assembly of spider silk proteins. In addition, support for a conserved, C-terminal cysteine residue participating in the formation of higher aggregate complexes through intermolecular disulfide bond linkages has been implied. In particular, recombinant MaSp C-terminal sequences have been shown to


form dimers under nonreducing conditions, whereas similar structured MiSps lacking the conserved cysteine residues fail to form higher-aggregate complexes. In addition to the C-terminal region playing an integral part of the liquid to crystalline phase transition, intrinsic chemical properties embedded within the primary sequence of silk fibroins have been demonstrated to display remarkable differences in their solubility and assembly characteristics. Comparative studies of the two major dragline silk proteins from *Araneus diadematus*, ADF-3 (MaSp2-like) and ADF-4 (MaSp1-like), demonstrate that ADF-3 is soluble at high concentrations [19], whereas ADF-4 is essentially insoluble and self-assembles into filamentous structures under certain experimental conditions [20]. A closer analysis of the hydropathicity demonstrates that ADF-4 is more hydrophobic in nature, which facilitates aggregation with other protein molecules. Interestingly, dragline silks have been found to contain pairs of proteins, which is a feature observed across a large number of spider species. Strikingly, different species display a common distinct distribution of hydrophobicity, with one protein being more hydrophilic (ADF-3/MaSp-2) and the other member more hydrophobic (ADF-4/MaSp1) [20].

Minor ampullate silks

Scanning electron microscopy demonstrates that minor ampullate silks form smaller-diameter fibers than do major ampullate silks. Two partial cDNAs that encode constituents of minor ampullate silk have been isolated from *N. clavipes*. These cDNAs encode two proteins named minor ampullate spidroin 1 and 2 (MiSp1 and MiSp2). Based upon mRNA lengths, the estimated protein size for MiSp1 is 320 kDa, whereas MiSp2 is 250 kDa. Southern blot analysis of genomic DNAs isolated from *N. clavipes* support the fact that these mRNAs are derived from two distinct genes [21]. Structurally, both proteins are organized into predominantly repetitive regions, with small non-repetitive C termini [21]. The highly repetitive regions consist mainly of alanine and glycine, with lower levels of tyrosine, glutamine and arginine being present. Gly-Gly-X and Gly-Ala repeats are significantly

represented throughout the primary amino acid sequence. Repetitive regions of both MiSp proteins are interrupted by ~137 amino acid serine-rich spacer regions; these spacer regions have similar serine composition relative to the amorphous region of *Bombyx mori*. Solution state conformational studies using Fourier transform infrared spectroscopy (FTIR) of minor ampullate silk collected from *N. edulis* demonstrate a dominant α -helical nature, with reduced β -sheet structure [22]. Solid-state NMR data suggest that the conformations of the alanine residues found in minor ampullate silk fibers are more heterogeneous in nature, with a large fraction present in a non- β sheet conformation [23]. The lower amount of β -sheet structure, yet high tensile strength of the fiber, suggests that minor ampullate silks may have different cross-linking mechanisms and matrix proteins, relative to major ampullate silks. From a mechanical perspective, minor ampullate silk is similar to major ampullate silk in tensile strength, but has lower elasticity [4].

Capture silks



Orb-weavers manufacture capture silks, which form the major component of the capture spiral of the web. Capture silk (flagelliform silk) has been proposed to consist largely of a single protein produced from the flagelliform gland, called Flag silk [24]. Partial cDNA sequences that encode for Flag silk have been retrieved, as well as extensive genomic DNA information. The *flag* gene represents the most extensively studied spider gene at the genomic DNA level. Characterization of the *flag* gene has demonstrated the presence of 13 exons that span over 30 kb of genomic DNA sequence. Flag transcripts have been determined by Northern blot analysis to be ~15 kb, with an estimated protein size of about 500 kDa [24]. Translation of the cDNA predicts a protein with multiple iterations, largely with the dominant repeat of this protein representing a pentapeptide Gly-Pro-Gly-Gly-X sequence, which can appear up to 63 times in tandem arrays [25]. Concatenated repeats of the Gly-Pro-Gly-Gly-X sequence have been proposed to form a β -spiral structure that can function as molecular ‘nanosprings’, which provide fiber elasticity. A second motif commonly found within the

predicted primary sequence represents the tripeptide Gly-Gly-X, which occurs approximately tenfold fewer times than Gly-Pro-Gly-Gly-X. The last repetitive flagelliform element, which is the longest and least abundant, represents a 28-amino-acid spacer region that is glycine poor. These motifs are woven together to form ensemble repeats that range from 368 to 411 residues. Comparison of the mechanical properties of the different silk types in orb web spiders demonstrates that Flag silks are the most extensible, but have lower tensile strength relative to dragline silk [6]. Within each monomeric protein, more than 14 ensemble repeats may be present. Both N and C-terminal sequence data demonstrate a nonrepetitive nature for Flag silk [25]. The Flag C terminus differs substantially from the primary sequences of the MaSp and MiSp silks, even though, presumably, these regions may perform similar functions. Although particular silk types in the same species have been found in pairs (e.g. MaSp1 and MaSp2), only one protein has been reported to assemble into flagelliform silks. Spidroins with similar functional properties likely exist in cobweb weavers. Although cob-weavers have been reported to lack capture silk, they have threads that are coated with glue-like substances. Instead of capture spirals, black widow spiders manufacture gumfooted lines that extend downward to the substrate from the supporting scaffolding of the cobweb, with only the bottom 5–15 mm being coated with aqueous glue [26]. Gumfooted lines may use structural related fibroins, but their molecular constituents remain to be determined.

Aciniform silks

Araneoid spiders use aciniform silks to wrap and immobilize prey, build sperm webs and web decorations. Relative to dragline silk amino acid compositions, which are rich in glycine and alanine, analyses of the luminal contents from aciniform glands have revealed low percentages of glycine and alanine. Evidence for the expression of a single silk fibroin gene that encodes an inferred protein closely matching the amino acid contents of the aciniform glands has been reported [27]. The predicted protein, aciniform spidroin 1 (AcSp1), displays a different structural organization relative to Flag, major ampullate and minor

ampullate silks. AcSp1 contains > 14 highly homogenized repeats, with each ensemble repeat consisting of 200 amino acid blocks; the repetitive sequences predicted from the AcSp1 cDNA do not resemble iterations found within other araneoid fibroins. Of the silk types studied in orb weavers, aciniform silks have lower tensile strength relative to dragline silks but higher extensibility and toughness [27]. The high degree of extensibility of aciniform silks is second only to flagelliform silks [6]. Phylogenetic analyses of the C-terminal aciniform sequence demonstrate that this fibroin groups weakly with major ampullate, minor ampullate and flagelliform silks, suggesting aciniform silks represent divergent members of the silk gene family.

Tubuliform silks

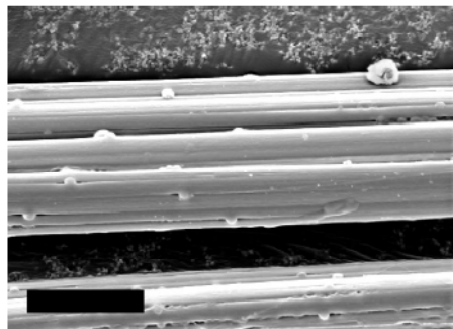


Fig 4: SEM image of a fiber of tubuliform silk.

Scanning electron microscope image of a fiber of tubuliform silk exhibiting characteristic grooves and nodules on its exterior. Bar, 5 μ m. (from [5])

Significant progress to unravel the structural and molecular properties of egg case (also known as tubuliform) silk has recently been reported. Aside from dragline silk, these threads represent the second most characterized spider silk at the molecular level. Egg case silk is produced by female spiders during the reproductive season. Scanning electron microscopy studies have revealed that spider egg cases contain two different diameter fibers in the cob-weaver, *Latrodectus Hesperus* [28], as well as the orb-weaver, *A. aurantia*. It has been suggested that the larger-diameter fibers are derived from the tubuliform gland, whereas the smaller-diameter fibers originate from the aciniform gland. Morphological studies indicate

that the tubuliform glands undergo structural changes prior to egg laying and egg case formation. Solid-state NMR and FTIR studies of egg case silks from *L. hesperus*, *A. diadematus* and *Achaearanea tepidariorum* demonstrate profound differences in their secondary structures. *A. tepidariorum* silk largely consists of α -helices and parallel β -sheets, whereas *A. diadematus* silk shows a more complex structure that also contains antiparallel β -strands and β -turns [29]. For *L. hesperus*, alanine residues are primarily found in a β -sheet environment [30]. The differences in these structures have been hypothesized to correlate with the different habitats of the spiders.

Some of the molecular constituents of egg case silk have recently begun to be elucidated. Denaturing polyacrylamide gel electrophoresis of egg case silk proteins from *N. clavata* have detected two proteins with sizes of 342 and 303 kDa [31], whereas a complex protein profile has been observed for *L. Hesperus* [28, 32]. One of the major components of the larger-diameter fiber has been determined at the molecular level; this protein represents tubuliform spidroin 1 (TuSp1). Analyses of the primary sequence of TuSp1 reveal large ensemble repeats that are ~184 amino acids in length, rich in serine, but low in glycine [30, 31]. TuSp1 orthologs have been isolated from a variety of different species (includes orb-weavers and cob-weavers) and their primary amino acid sequences are highly conserved across species. New amino acid motifs which include S_n , $(SA)_n$, $(SQ)_n$ and GX (X represents Q, L, Y, I, V and A) have been identified. Analysis of the primary sequence of *L. hesperus* TuSp1 reveals motifs that are potentially involved in β -sheet structure, which include the modules AAQAASAA, AAAQA and AASQAA. Relative to the polyalanine blocks found in major ampullate silks, these motifs contain larger side chain groups that are more hydrophilic in nature (Q and S). The bulkier side chains of serine and glutamine are consistent with the larger side chain spacing detected in the β -sheet regions by X-ray diffraction studies of egg case silks from *N. clavipes*.

Comparison of the C terminus of TuSp1 with other silk family members demonstrates a

highly divergent silk fibroin family member. Based upon this lack of similarity, TuSp1 has been proposed to represent an evolutionary ancient silk. Real-time PCR analysis has confirmed the tubuliform gland-restricted mRNA expression pattern for TuSp1, whereas matrix-assisted laser desorption ionization (MALDI) tandem time-of-flight (TOF) mass spectrometry of peptides generated from tryptic digestion of solubilized egg case material provides direct evidence for the assembly of TuSp1 into the fiber [30]. Digestion of the egg case core fiber with trypsin, followed by the analysis of the peptides using MALDI tandem TOF MS, has led to the discovery of two other proteins that are assembled into the core fiber of *L. hesperus*, egg case protein 1 and 2 (ECP-1 and ECP-2) [28, 33]. Although the core fiber of dragline silk is presumably dimeric in nature, the core fiber of egg case silk has been demonstrated to represent a trimeric complex, consisting of TuSp1, ECP-1 and ECP-2 [33]. Similar to the mRNA expression profile for TuSp1, the ECPs also display tubuliform-restricted patterns of expression. Real-time PCR analysis indicates that TuSp1 mRNA levels are approximately 20-fold higher relative to the ECPs [33]. This suggests that the ECPs represent lower-abundance species in the egg case fiber. Analyses of the ECP primary sequences indicate that they share similarity to fibroins from spiders and silkworms, with short polyalanine and poly(Gly-Ala) modules. The ECPs show extreme codon biasness at the wobble position (A or U), similar to other fibroins, as well as constituting a pair of proteins, which is a common feature in the spidroin family (e.g. MaSp1 and MaSp2) [28]. Similar to TuSp1 and AcSp1, the ECPs lack the conserved, nonrepetitive C termini, which is characteristic for some fibroin family members. Perhaps more intriguing is the primary sequence of their N termini, which contain 16 conserved cysteine residues. Evidence that these residues mediate higher-aggregate complex formation, presumably by intermolecular disulfide bond linkages, is supported by their increased monomeric accumulation after prolonged treatment of solubilized egg case material with reducing agents [28]. Collectively, these data suggest the ECPs may function as intermolecular crosslinkers, with potential

structural roles in the egg case fiber. It will be interesting to determine whether ECP-like molecules are present in orb-weavers or more divergent spider species.

Glue and pyriform silks

No cDNAs encoding proteins that represent glue or pyriform silks have been reported. Comparatively little is known about these silks types. Amino acid compositions have been determined for both silks using luminal gland materials from orb-weavers. Pyriform and aggregate silks contain very polar amino acids, which include Ser, Asp, Glu, Thr, Lys and Arg [34]. Although the precise molecular identities of the proteins involved in both silks/glues remain to be determined, the aggregate glands have been shown to produce a glycoprotein coating that likely provides stickiness to the capture silk fiber.

1.3 : Study for forming spider silk

The processing of water soluble high molecular weight silk proteins into water insoluble fibers in both spider and silkworm involves many factors including disulfide bond formation, cation interactions, glycosylation and perhaps other chemical or physical steps (Kaplan et al., 1992a,b). Initially, some degree of self-organization or assembly drives the formation of the crystalline repeats in the protein fibers. In the silkworm, changes in physiological conditions such as pH and salt concentrations in the gland accompany the processing and presumably help maintain solubility despite increasing protein concentration during passage through the various regions. Physical shear generated during spinning the soluble silk appears in a large part responsible for conversion to the insoluble silk fiber in the natural spinning process (Ilzuka 1985a,b; Magoshi et al., 1985, 1994). In the spider and silkworm there are three distinct regions to the glands and two sets of these organs feeding into one final thread (Magoshi et al., 1985, 1994; Tillinghast and Townley, 1994). In the silkworm the protein concentration is approximately 20~30% in the middle region of the gland where the fibroin is stored and sericin is synthesized, and significantly higher in the

anterior region of the gland where spinning is initiated (Magoshi et al., 1985, 1994). In the spider the dragline protein is synthesized in the pair of major ampullate glands. Depending on environmental conditions and needs, the amino acid composition of the silk can vary considerably, not only between individual spiders but also for the same spider on different days (Work and Young, 1987; Vollrath, 1999) [35], which raises questions about the genomic sequences and organization of the genes encoding these proteins. Compared to the silkworm, the major ampullate gland in the spider is smaller and there is no sericin contribution in the middle region of the gland. The process leads to the formation of a lyotropic liquid crystalline phase prior to spinning in both the spider and the silkworm, and in many of the different glands of the spider responsible for the different silks (Kerkam et al., 1991; Viney et al., 1994). The formation of this liquid crystalline phase is characterized by axial alignment and interaction of polymer chains in various stages of registry with each other while remaining soluble in aqueous medium. This is one method that allows the spider to maintain a relatively high concentration of the protein in aqueous solution prior to spinning without resulting in the formation of insoluble β -sheets.

Solubilization of spun spider silks is difficult. Most solvents used to solubilize globular proteins will not suffice. The highly organized fibrous structure of silk and the extensive hydrogen bonding and van der Waals interactions lead to the exclusion of water from the intersheet regions of the β -sheets after spinning. Silk fibers are insoluble in water, dilute acids and alkali, chaotropic agents such as urea and guanidine hydrochloride and most organic solvents (Lombardi and Kaplan, 1990; Mello et al., 1994). The silks are also resistant to most proteolytic enzymes, with chymotrypsin an exception for silkworm fibroin. Spider silk can be solubilized by immersion of the fibers in very high concentration salt solutions such as lithium bromide, lithium thiocyanate or calcium chloride and other calcium salts. Also high concentrations of propionic acid/hydrochloric acid mixtures and formic acid can be used (Mello et al., 1994). After solubilization, dialysis into chaotropic agents, water or buffers can

be carried out; however, rapid reprecipitation or gelation is a common result. This aggregation is mostly due to the formation of beta-sheet conformations. Solid state ^{13}C -NMR and ^2H -NMR studies of *N. clavipes* dragline silk indicate that the crystalline fractions are composed primarily of alanine rich-sequences, including highly oriented regions (Simmons et al., 1994, 1996). The crystalline polyalanine regions are not affected by water while the other domains are plasticized leading to supercontraction and shrinkage of the major ampullate dragline silk from *N. clavipes* (Jelinski et al., 1999).

Thin films have been prepared from silk proteins (Muller et al., 1993) and a silk conformation (silk III)(secondary structure with a diffraction pattern that matches a polyglycine 3_1 -helical structure) have been observed depending on the conditions used to prepare the silk protein (Valluzzi et al., 1996). These hexagonally packed threefold helices were observed by electron diffraction analysis of the thin films after transfer to transmission electron microscopy grids. Cholesteric liquid crystalline phases have been observed with the protein based on observations in situ after cryogenic quenching and microtoming of actively spinning *N. clavipes* and *B. mori*, followed by TEM, electron diffraction and AFM characterization (Willcox et al., 1996) [36]. Correlations between primary silk primary sequence and self-assembly at air-water and organic solvent- water interfaces are providing insight into the processing options for these types of proteinbased materials to ‘direct’ the assembly in a desired path of secondary and higher-order structure formation (Valluzzi et al., 1999a,b; Wilson et al., 2000).

Unlike man-made fibers, the silks of spiders are spun from aqueous solutions and at atmospheric pressure in a process still poorly understood. The molecular mechanism of this process involves the conversion of a highly concentrated, predominantly disordered silk protein (spidroin) into β -sheet-rich structures.

Spidroins, the major silk proteins making up the spider’s dragline silk, originate in two distinct tissue layers (A and B) in the spider’s major ampullate gland. Earlier studies indicate

that the lumen in the tail and ampulla A zone portions are slightly alkaline or neutral whereas the B zone and duct are acidic (see Fig. 5~7). The origin of this pH gradient in the ampulla is not clear, nor has the gradient been fully quantified, though several hypotheses have been put forward. The secretion of acidic polysaccharides in the B zone and the presence of a high concentration of tyrosine residues in the A zone and tail might account for variation in pH (see Fig.5). A high activity of phosphatases in epithelial cells suggests that pH may be influenced by the secretion of phosphate ions into the lumen of the gland. More recently, the amino acid composition and the partial DNA sequences of spider silk proteins indicate the presence of residues such as histidine, arginine, glutamate/glutamine, and aspartate/asparagine that could influence the pH.

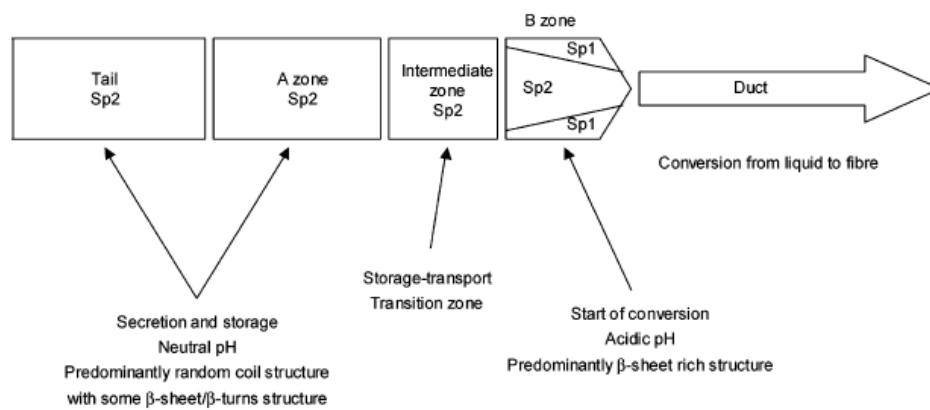


Fig 5: Spinning pathway of spider.

Flow chart summarizing the correlation between pH and the structure along the spinning pathway (the shape of the B-zone box represents the narrowing of the B-zone in the gland). (from [37])

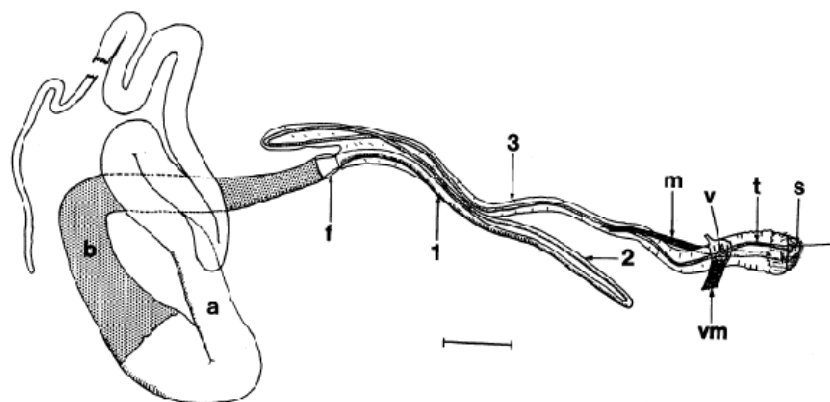


Fig 6: Drawing of dissected major ampullate gland and associated structures taken from a light micrograph. a, A-zone; b, B-zone; f, funnel; 1,2,3, first, second and third limbs of duct; m, duct levator muscle; v, valve; vm, valve tensor muscle; t, terminal tubule; s, spigot, Scale bar 1mm. (from [38])

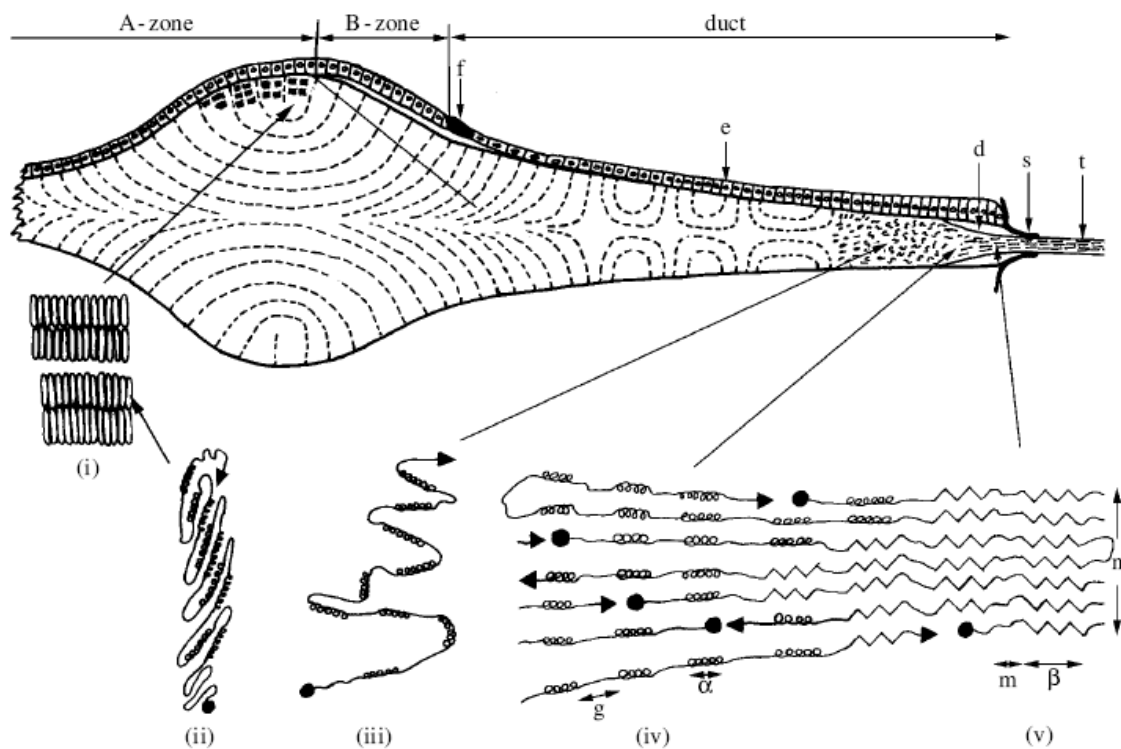


Fig 7: The proposed stages in lamellar liquid crystalline assembly of the nano fibrils of the major ampullate (dragline) silk thread in orb web spiders (see text) showing.

The proposed stages in lamellar liquid crystalline assembly of the nano fibrils of the major ampullate (dragline) silk thread in orb web spiders (see text) showing: (i) a diagrammatic of the gland and duct (upper part of illustration); nematic discotic units; (ii) rod-shaped molecules of spidroin; (iii) partly unwound molecules; (iv) early stage of formation of the solid fibre and (v) fully formed fibre (see text). The lumen of the gland has been represented as much wider in proportion to length with only a small number of bi-layer discs (top left) and the epithelium, (e), only on one side of the duct and gland. The dotted lines represent the molecular director field. This lies at right angles to the slow axis of polarization as a result of the assembly of the compactly wound, rod-shaped molecules of spidroin (ii) into bi-layered discs of the nematic discotic phase (i). These are present as an escaped nematic texture in the gland proper and first half of the duct (upper half of figure). Funnel (f), draw down taper (d), spigot (s), thread (t), glycine-rich segments (g), polyalanine segments (a), mobile segments (m), bcrySTALLITES (b), nano fibrils (n). Based on Knight & Vollrath (1999), Vollrath & Knight (2001), Knight & Vollrath (2001a,b) and Chen et al. (2001). (From Phil. Trans. Soc. Lond. B (2002) 357, 155~163)

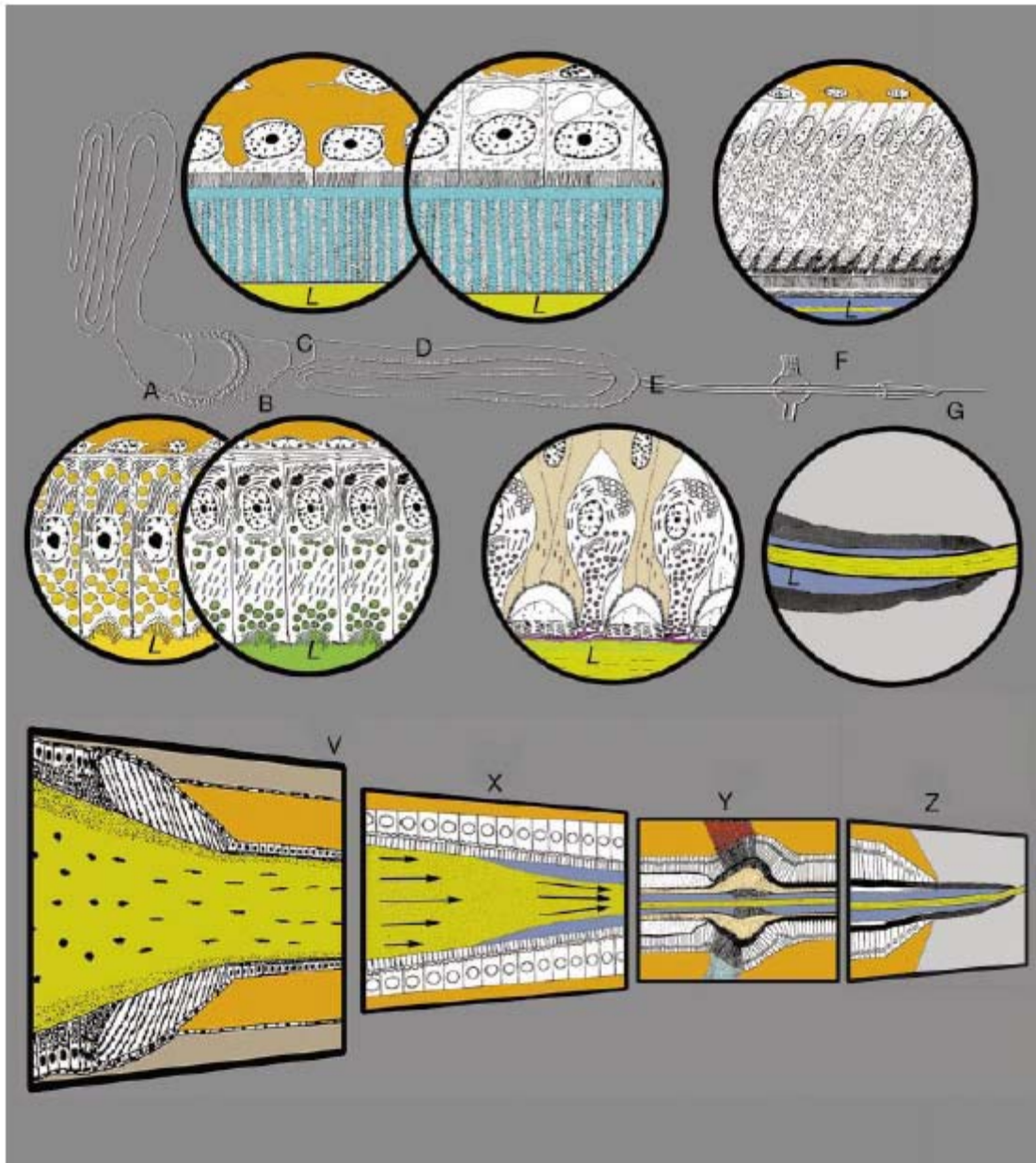


Fig 8: A spider's dragline spinneret.

A spider's dragline spinneret. The top part shows original drawings of the histology of the spinneret (lumen, L); the bottom part outlines its spinning function, which entails drawing the liquid crystalline dope solution produced in the gland through a tapering s-shaped duct, thereby converting it into an elastic thread. Dope production occurs in two zones: the A-zone of the gland (see panel A) secretes spidroin, the protein forming the core of the thread, while the B-zone (see panel B) secretes the thread's thin coat. The secretory vesicles of the A-zone contain short, narrow filaments; most of those of the B-zone contain hexagonal columnar liquid crystals. The greatly thickened cuticle of the funnel (in panel V) anchors the extensible duct to the less mobile sac, perhaps to prevent shearing of the dope when the spider wiggles. The duct itself has a thin cuticle, which acts as a dialysis membrane and may allow water and sodium ions out of the lumen, and potassium ions, surfactants and lubricants into the lumen to facilitate thread formation (see panel X). The epithelium of the s-shaped duct progressively increases in height from the funnel to the valve, suggesting increased pumping of water and ions as

the dope is drawn through the duct (panels C and D show the histology of epithelium in the first and second limbs, respectively). The drawdown process is mainly internal and starts in the third limb of the duct (see panel X), approximately 4mm from the exit spigot. Just before and after the start of the drawdown taper, single flask-shaped gland cells, such as seen in inset E, may contribute an extra coating to the thread. The 'valve', shown in panel Y in the bottom of the figure, is not a restriction nozzle, but a clamp for gripping the thread. It may also act as a 'ratchet' or 'pump', to restart spinning after internal rupture of a filament. The section of duct (see inset F) after the valve appears to be highly specialized for water pumping, having tall cells with numerous mitochondria and apical microvilli and a large surface area provided by apical infoldings of the plasma membrane. Finally, the thread is gripped by the flexible and elastic lips of the spigot (inset G), through which it passes to the outside world (see panel Z). The spigot strips off the last of the aqueous phase surrounding the thread, thus helping to retain water in the spider, and also places the thread under tension for the final air-drawing step. (from [34])

1.4 : Application of protein as self-assembled motif to

produce nanostructure



There are many researches about using designed peptide to self-assembled into protein nanostructure. Let us take some example for these special structures by biomolecules.

Chuncaai Zhou, et al synthesized two hybrid multiblock copolymers by condensing poly(alanine) [(Ala)₅] blocks of the structural proteins (spidroin MaSp1 and MaSp2) of spider dragline silk with different oligomers of isoprene (2200 and 5000 Da) having reactive end groups. The synthetic multiblock polymer displayed similar secondary structure to that of natural spidroin, the peptide segment forming a β -sheet structure (see Fig. 9).[39]

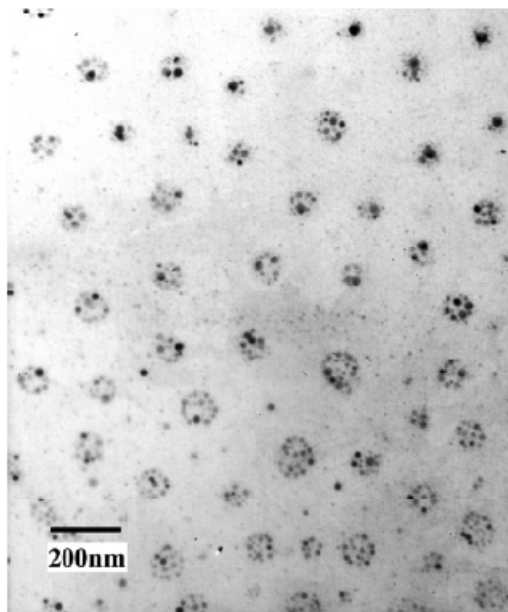


Fig 9: TEM image of unstained film prepared from 0.001% PEP-PI2200 copolymer in 2:1 v/v $\text{CHCl}_3/\text{HOCH}_2\text{CH}_2\text{Cl}$.

TEM image of unstained film prepared from 0.001% PEP-PI2200 copolymer in 2:1 v/v $\text{CHCl}_3/\text{HOCH}_2\text{CH}_2\text{Cl}$. This is thought to show a micellar-like aggregation. (from [39])

Ramin Djalali, et al used sequenced peptide nanotubes as templates to fabricate Au nanowires (see Fig. 10).[40] They also demonstrated that monodisperse Au nanocrystals were synthesized inside the cavities of peptide nano-doughnuts by the reduction of Au ions and the size of the Au nanocrystal was controlled by the cavity dimension (see Fig. 11).[41]

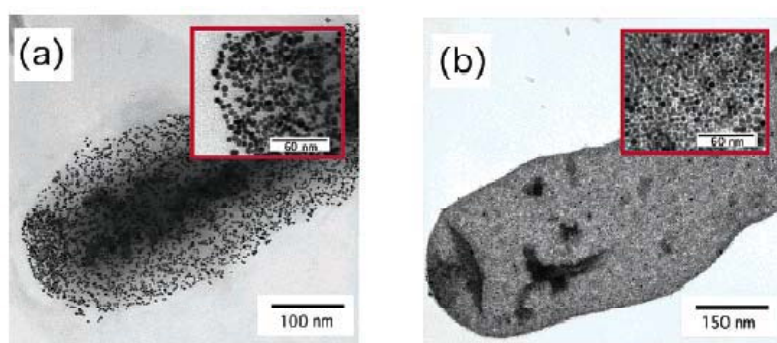


Fig 10: TEM images of Au nanocrystals on the sequenced histidine-rich peptide nanotubes.

TEM images of Au nanocrystals on the sequenced histidine-rich peptide nanotubes grown by reducing the Au ion-nanotube solution after incubating Au ions for 10 days at (a) pH = 8 (b) pH = 11.5. Insets show the TEM images in higher magnification.(from [40])

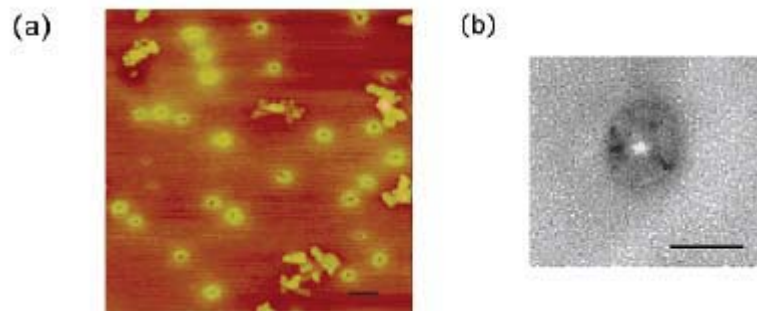


Fig 11: SFM image of the peptide nano-doughnuts.

(a) SFM topographic image of the peptide nano-doughnuts. Scale bar = 100 nm. (b) TEM image of the peptide nano-doughnut. Scale bar = 50 nm. (from [41])

Mudalige Thilak Kumara, et al applied *E. coli* flagellin protein (FliTrx) to form self-assembling protein nanotube (see Fig. 12).[42]

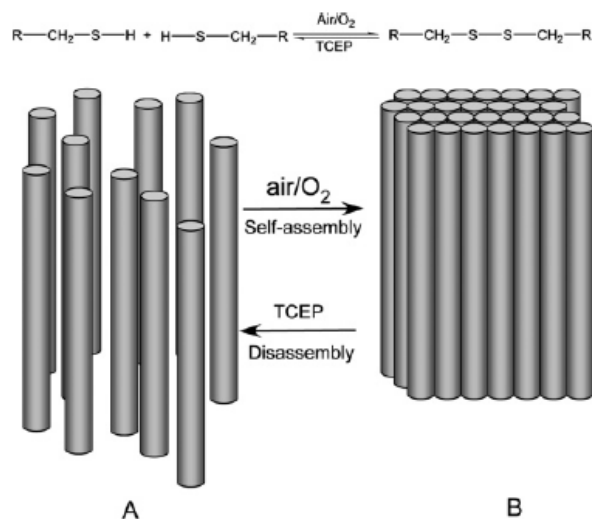


Fig 12: Model for flagella nanotube self-assembly and disassembly.

(A) Formation of disulfide bonds between cysteine loops in the presence of oxygen. (B) Flagella nanotube bundle formation upon oxidative disulfide bond formation and disassembly upon addition of a reducing agent. (from [42])

Ohad Carny, et al demonstrate the devise of metal-insulator-metal, trilayered, coaxial nanocables. Such coaxial geometry may give rise to useful and unique electromagnetic properties. We have fabricated these nanostructures using a scaffold of self-assembled peptide nanotubes. Gold nanoparticles were bound to the surface of peptide nanotubes via a common molecular recognition element that was included in various linker peptides. This enabled us to promote site-specific metal reduction and to create the coaxial nanostructure (see Fig.

13,14).[43]

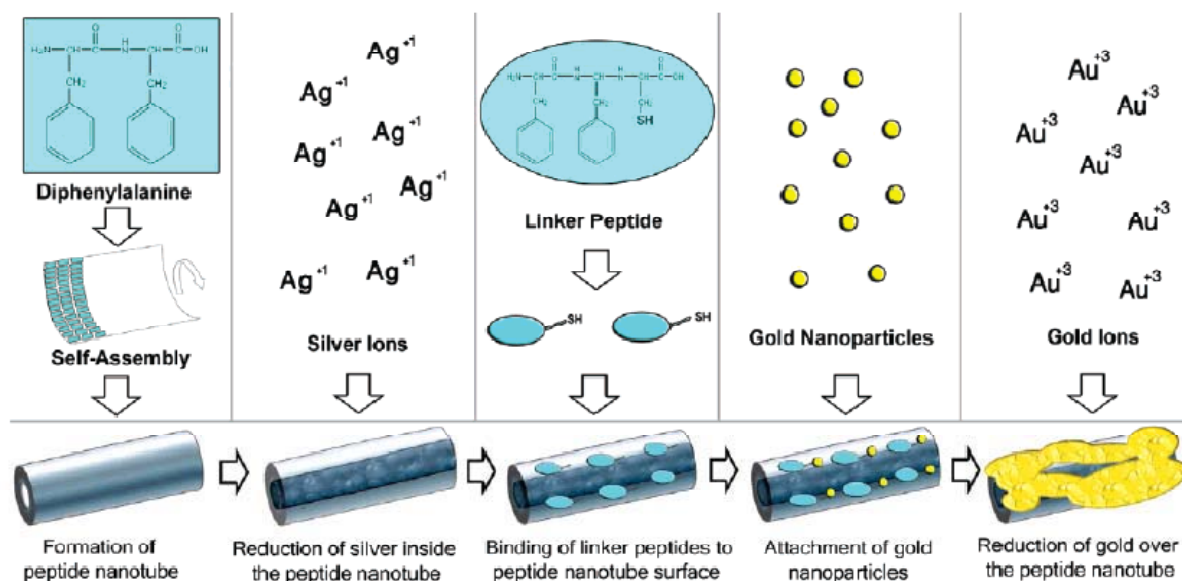


Fig 13: Model for fabricating a coaxial nanowire.

Model for fabricating a coaxial nanowire. A model diagram describing (from left to right) the self-assembly of the peptide nanotube; reduction of silver in the hollow pore of the peptide nanotube; binding of linker peptide nanotube surface; attachment of gold nanoparticles; and electroless deposition of a gold cover the peptide nanotube using the bonded gold nanoparticles as nucleation sites. (from [43])

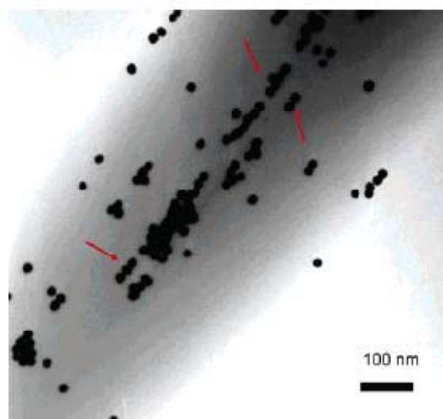


Fig 14: Ordered organization of the nanoparticles on the nanotubes.

Ordered organization of the nanoparticles on the nanotubes. The red arrows in the TEM image denote “lines” of bounded particles. This indicates that the peptide nanotubes’ assemblies have some level of ordered organization. (from [43])

Osman Rathore and Dotsevi Y. Sogah used selective replacement of the amorphous peptide domain of a spider silk with poly(ethylene glycol) gave *N. clavipes* silk-inspired polymers having similar solid-state structures and very good mechanical properties. The

tendency of poly(alanine) having appropriate chain length to form β -sheets and the facility with which the β -sheets self-assemble have been retained in the polymers (see Fig. 15).[44]

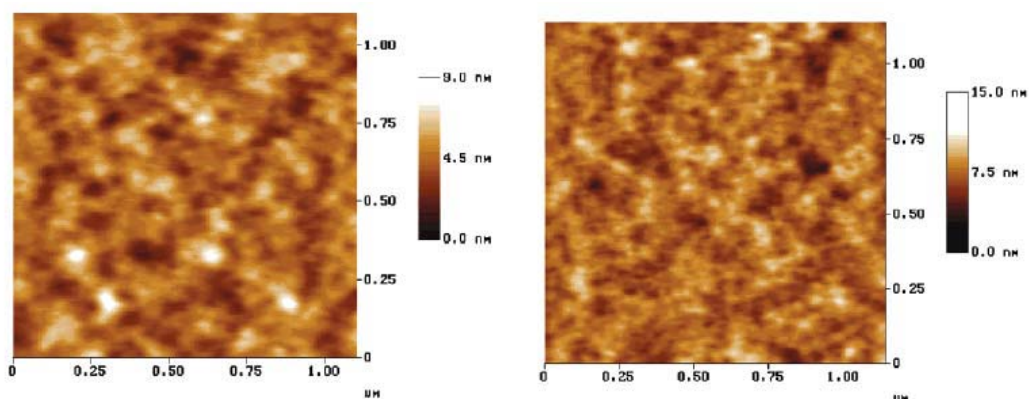


Fig 15: Tapping mode AFM topographical plots of (Ala)₄ (left image) and (Ala)₆ (right image) spin-coated film on a silicon wafer. (from [44])

Amit Singh, Shantesh Hede, and Murali Sastry showed that spider silk is an excellent scaffold for the one-step synthesis and assembly of gold nanoparticles (see Fig. 16).[45]

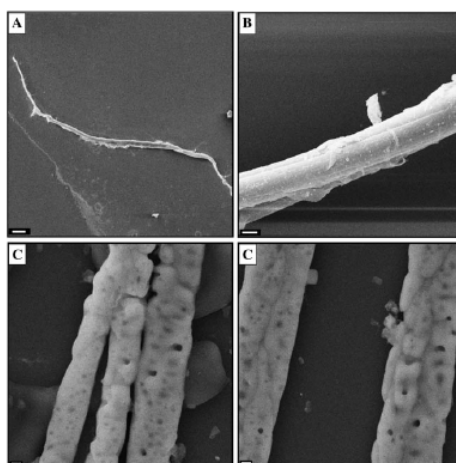


Fig 16: SEM images of spider silk as scaffold for the one-step synthesis and assembly of gold nanoparticles. (A,B) Representative SEM images from a spider-like fiber at different magnifications. The scale bar in A and B correspond to 30 and 3 μm , respectively. (C,D) Representative SEM image at different magnifications recorded from a spider-like fiber after exposure to a 10^{-1} M aqueous solution of chloroauric acid for 48 hr. The scale bars in both the images correspond to 1 μm . (from [45])

Katharina Janek, et al present water-soluble de novo β -sheet peptides which self-assemble into fibrillar structures. The model peptides enable studies of the relationship between β -sheet stability and association behavior. The peptides [DPKGDPKG-(VT)*n*-GKGDPKPD-NH₂, *n* = 3-8] are composed of a central β -sheet-forming

domain (VT-sequence), and N- and C-terminal nonstructured octapeptide sequences which promote water solubility (see Fig. 17).[46]

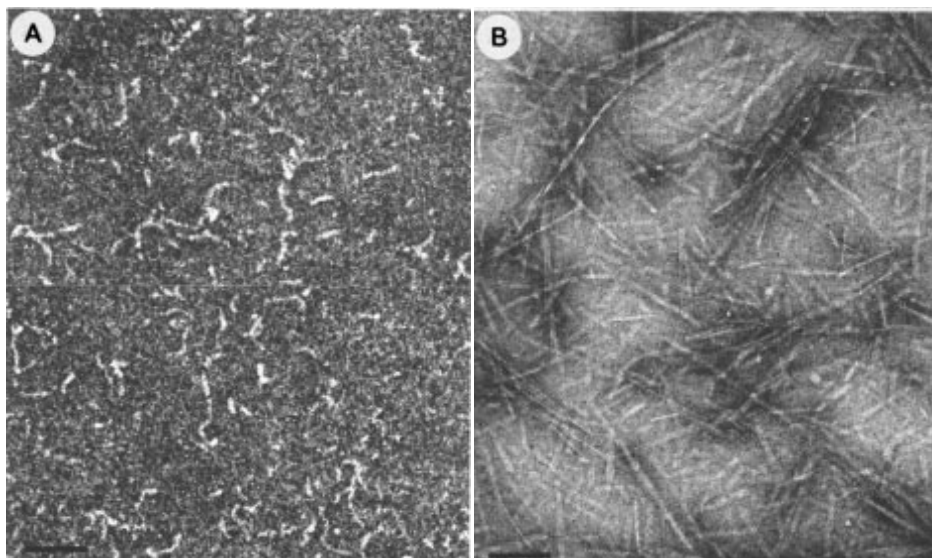
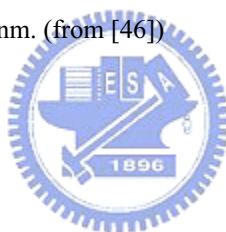


Fig 17: Electron micrographs of negatively stained (2% uranyl acetate) fibrils.

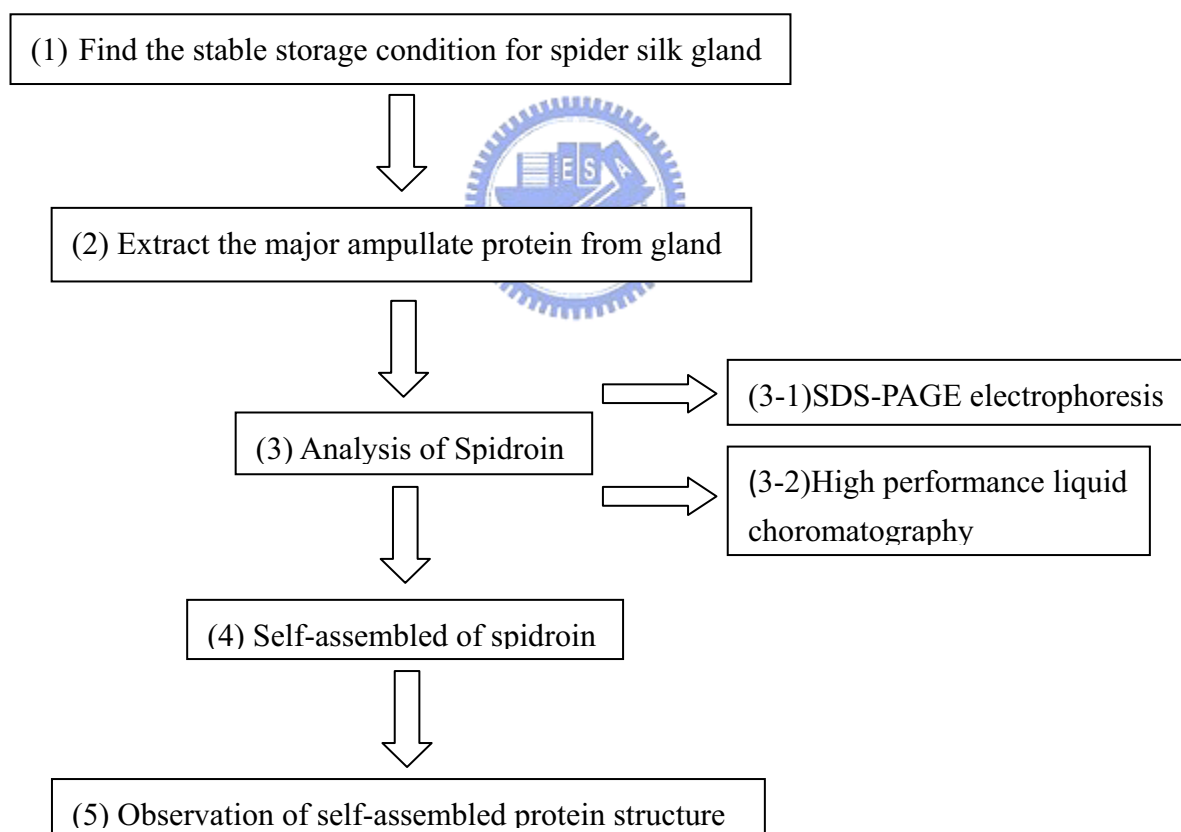
Electron micrographs of negatively stained (2% uranyl acetate) fibrils from an aqueous solution (2×10^{-4} M) of peptide VT8 (A) and VT8-DD (B). Bar, 100 nm. (from [46])



Chapter 2 : Experiment Design, Materials and Methods

2.1 : Experiment Design

The first problem we need to solve was how to let spider major silk gland storage stably. We designed a series of physiological parameters, such as pH, ions and temperature etc. We also need to purify our spidroin for further study. Spidroin were analyzed by SDS-PAGE electrophoresis and gel-filtration column. When we had basic understanding of our spidroin, we tried some physiological parameters to self-assemble the spidroin. Finally, the SAMs were observed by scanning electron microscopy.



2.2 : Chemicals

All chemicals, which were of analytical grade or higher, were obtained from Sigma Chemical Co. (St. Louis, MO) or Merck (Darmstadt, Germany).

2.2.1 : Spider species

Major ampullate gland proteins of mature female *Nephila pilipes* were used in this study. The major ampullate gland was storage in Buffer I and dissolved the major ampullate gland proteins overnight to obtain our spidroin. The proteins were filtered with 0.25um filter before use.



Fig 18: The photograph is a mature female *Nephila pilipes*.

2.2.2 : Stable buffer for Spidroin

Storage Buffer I:

Chemical	Final Concentration
Urea	2M
2-mercaptoethanol	10mM
Ethylenediaminetetraacetic acid	3mM
Phenylmethanesulfonyl fluoride	1mM
NaH ₂ PO ₄ · H ₂ O	10mM

Ringer Solution: (pH 8.2)

NaCl	13.03g
KCl	0.51g
CaCl ₂	0.89g
MgCl ₂ · 6H ₂ O	1.04g

2.2.3 : SDS-PAGE chemicals

Separating Gel:

Composition \ Percentage of separating gel	6%	8%	10%	12%	15%
H ₂ O	5.35 ml	4.68 ml	4 ml	3.35 ml	2.35 ml
1.5M Tris-HCl (pH=8.8)	2.5 ml	2.5 ml	2.5 ml	2.5 ml	2.5 ml
40% Acrylamide-Bis	2 ml	2.67 ml	3.35 ml	4 ml	5 ml
10% SDS	100 ul	100 ul	100 ul	100 ul	100 ul
10% APS	50 ul	50 ul	50 ul	50 ul	50 ul
TEMED	10 ul	10 ul	10 ul	10 ul	10 ul

Stacking Gel:

Composition \ Percentage of stacking gel	4%
H ₂ O	3.05 ml
0.5M Tris-HCl (pH=6.8)	1.25ml
40% Acrylamide-Bis	650 ul
10% SDS	50 ul
10% APS	25 ul
TEMED	10 ul

10X Running Buffer:

Tris-Base 30.3g, Glycine 144g, and SDS 10g, and add deionized water to 1L.

Tris-Base	30.3g
Glycine	144g
SDS	10g

Then, add deionized water to 1L.

5X Sample buffer:

Deionized water	4.0ml
0.5M Tris-HCl (pH6.8)	1.7ml
Glycerol	5.0ml
20% SDS	0.5ml
2-mercaptoethanol	2.0ml
Bromophenol Blue	6mg

Gel Stain-Coomassie Blue:

coomassie Blue	1.5 g
methanol	500ml
ddH ₂ O	500ml
acetic acid	100ml

Dissolve coomassie Blue in methanol first.

Destain I:

Methanol	400ml
Acetic acid	100ml
ddH₂O	500ml

Destain II:

Methanol	50ml
Acetic acid	120ml
ddH₂O	880ml

2.2.4 : High performance liquid chromatography

Phosphate buffer saline (PBS) :

NaCl	8g
Na ₂ HPO ₄	1.44g
KCl	0.2g
KH ₂ PO ₄	0.24g

Then, add deionized water to 1L, adjust pH to 7.0, and filtered with 0.25 μ m filter.

2.2.5 : Electron microscopy fixation and dehydration chemicals

Preparation of 2% tannic acid solution:

2g Tannic acid add to 100ml DI water.

Preparation of 1.25% Glutaraldehyde fixation solution (contained tannic acid):

Add 25% Glutaraldehyde solution 10ml, Tannic acid 90ml, PBS 100ml. Final concentration of Glutaraldehyde solution = 1.25%. Adjust pH to 7.4.

Preparation of Osmium tetroxide postfixation solution (OsO₄):

Add 25%OsO₄ 10ml, DI water 10ml, PBS 20ml.

100% HMDS (Hexamethyldisizane)

2.3 : Instruments

2.3.1 : SDS-PAGE electrophoresis

SDS-PAGE stands for Sodium dodecyl sulfate (SDS) polyacrylamide gel electrophoresis (PAGE) and is a method used to separate proteins according to their size. Since different proteins with similar molecular weights may migrate differently due to their differences in secondary, tertiary or quaternary structure, SDS, an anionic detergent, is used in SDS-PAGE to reduce proteins to their primary (linearized) structure and coat them with uniform negative charges.

Procedures for SDS-PAGE generally involve:

1. Making a gel and assembling the gel apparatus.
2. Mixing protein samples with sample buffer containing SDS and heat the mixture at high temperature.
3. Loading samples and running the electrophoresis.
4. Fixing and staining the separated proteins.

2.3.2 : High-performance liquid chromatography

The High Performance Liquid Chromatography system consisted of one L-2100 pump, L-2200 Autosampler, and L-2450 diode array detector all from Hitachi (Tokyo, Japan). Separations were performed on a SynChropak GPC 4000 column (250 × 4.6 mm, Eprogen Inc.).

High-performance liquid chromatography (HPLC) is a form of column chromatography used frequently in biochemistry and analytical chemistry. HPLC is used to separate components of a mixture by using a variety of chemical interactions between the substance being analyzed the chromatography column.

In isocratic HPLC the analyte is forced through a column of the stationary phase (usually a tube packed with small round particles with a certain surface chemistry) by pumping a liquid (mobile phase) at high pressure through the column. The sample to be analyzed is introduced in a small volume to the stream of mobile phase and is retarded by specific chemical or physical interactions with the stationary phase as it traverses the length of the column. The amount of retardation depends on the nature of the analyte, stationary phase and mobile phase composition. The time at which a specific analyte elutes (comes out of the end of the column) is called the retention time and is considered a reasonably unique identifying characteristic of a given analyte. The use of pressure increases the linear velocity (speed) giving the components less time to diffuse within the column, leading to improved

resolution in the resulting chromatogram. Common solvents used include any miscible combinations of water or various organic liquids (the most common are methanol and acetonitrile). Water may contain buffers or salts to assist in the separation of the analyte components, or compounds such as Trifluoroacetic acid which acts as an ion pairing agent.

A further refinement to HPLC has been to vary the mobile phase composition during the analysis, this is known as gradient elution. A normal gradient for reverse phase chromatography might start at 5% methanol and progress linearly to 50% methanol over 25 minutes, depending on how hydrophobic the analyte is. The gradient separates the analyte mixtures as a function of the affinity of the analyte for the current mobile phase composition relative to the stationary phase. This partitioning process is similar to that which occurs during a liquid-liquid extraction but is continuous, not step-wise. In this example, using a water/methanol gradient, the more hydrophobic components will elute under conditions of relatively high methanol; whereas the more hydrophilic compounds will elute under conditions of relatively low methanol. The choice of solvents, additives and gradient depend on the nature of the stationary phase and the analyte. Often a series of tests are performed on the analyte and a number of generic runs may be processed in order to find the optimum HPLC method for the analyte - the method which gives the best separation of peaks.

2.3.2.1 : Normal phase chromatography

Normal phase HPLC (NP-HPLC) was the first kind of HPLC chemistry used, and separates analytes based on polarity. This method uses a polar stationary phase and a nonpolar mobile phase, and is used when the analyte of interest is fairly polar in nature. The polar analyte associates with and is retained by the polar stationary phase. Adsorption strengths increase with increase in analyte polarity, and the interaction between the polar analyte and the polar stationary phase (relative to the mobile phase) increases the elution time. The

interaction strength not only depends on the functional groups in the analyte molecule, but also on steric factors and structural isomers are often resolved from one another. Use of more polar solvents in the mobile phase will decrease the retention time of the analytes while more hydrophobic solvents tend to increase retention times. Particularly polar solvents in a mixture tend to deactivate the column by occupying the stationary phase surface. This is somewhat particular to normal phase because it is most purely an adsorptive mechanism (the interactions are with a hard surface rather than a soft layer on a surface).

NP-HPLC had fallen out of favor in the 1970's with the development of reversed-phase HPLC because of a lack of reproducibility of retention times as water or protic organic solvents changed the hydration state of the silica or alumina chromatographic media. Recently it has become useful again with the development of HILIC bonded phases which utilize a partition mechanism which provides reproducibility.



2.3.2.2 : Reversed Phase chromatography

Reversed phase HPLC (RP-HPLC) consists of a non-polar stationary phase and a moderately polar mobile phase. One common stationary phase is a silica which has been treated with RMe_2SiCl , where R is a straight chain alkyl group such as $\text{C}_{18}\text{H}_{37}$ or C_8H_{17} . The retention time is therefore longer for molecules which are more non-polar in nature, allowing polar molecules to elute more readily. Retention time is increased by the addition of polar solvent to the mobile phase and decreased by the addition of more hydrophobic solvent. Reversed phase chromatography is so commonly used that it is not uncommon for it to be incorrectly referred to as "HPLC" without further specification.

RP-HPLC operates on the principle of hydrophobic interactions which result from repulsive forces between a relatively polar solvent, the relatively non-polar analyte, and the non-polar stationary phase. The driving force in the binding of the analyte to the stationary phase is the decrease in the area of the non-polar segment of the analyte molecule exposed to the solvent. This hydrophobic effect is dominated by the decrease in free energy from entropy associated with the minimization of the ordered molecule-polar solvent interface. The hydrophobic effect is decreased by adding more non-polar solvent into the mobile phase. This shifts the partition coefficient such that the analyte spends some portion of time moving down the column in the mobile phase, eventually eluting from the column.

The characteristics of the analyte molecule play an important role in its retention characteristics. In general, an analyte with a longer alkyl chain length results in a longer retention time because it increases the molecule's hydrophobicity. Very large molecules, however, can result in incomplete interaction between the large analyte surface and the alkyl chain. Retention time increases with hydrophobic surface area which is roughly inversely proportional to solute size. Branched chain compounds elute more rapidly than their corresponding isomers because the overall surface area is decreased.

Aside from mobile phase hydrophobicity, other mobile phase modifiers can affect analyte retention. For example, the addition of inorganic salts causes a linear increase in the surface tension of aqueous solutions, and because the entropy of the analyte-solvent interface is controlled by surface tension, the addition of salts tend to increase the retention time. Another important component is pH since this can change the hydrophobicity of the analyte. For this reason most methods use a buffering agent, such as sodium phosphate to control the pH. An organic acid such as formic acid or most commonly trifluoroacetic acid is often added to the mobile phase. These serve multiple purposes: They control pH, neutralize the charge on any residual exposed silica on the stationary phase and act as ion pairing agents to neutralize

charge on the analyte. The effect varies depending on use but generally improve the chromatography.

Reversed phase columns are quite difficult to damage compared with normal silica columns, however, many reverse phase columns consist of alkyl derivatized silica particles and should never be used with aqueous bases as these will destroy the underlying silica backbone. They can be used with aqueous acid but the column should not be exposed to the acid for too long, as it can corrode the metal parts of the HPLC equipment. The metal content of HPLC columns must be kept low if the best possible ability to separate substances is to be retained. A good test for the metal content of a column is to inject a sample which is a mixture of 2,2'- and 4,4'- bipyridine. Because the 2,2'-bipy can chelate the metal it is normal that when a metal ion is present on the surface of the silica the shape of the peak for the 2,2'-bipy will be distorted, tailing will be seen on this distorted peak.

2.3.2.3 : Size Exclusion chromatography



Size exclusion chromatography (SEC) is a chromatographic method in which particles are separated based on their size, or in more technical terms, their hydrodynamic volume. It is usually applied to large molecules or macromolecular complexes such as proteins and industrial polymers. When an aqueous solution is used to transport the sample through the column, the technique is known as gel filtration chromatography. The name gel permeation chromatography is used when an organic solvent is used as a mobile phase. The main application of gel filtration chromatography is the fractionation of proteins and other water-soluble polymers, while gel permeation chromatography is used to analyze the molecular weight distribution of organic-soluble polymers.

SEC is a widely used technique for the purification and analysis of synthetic and biological polymers, such as proteins, polysaccharides and nucleic acids. Biologists and biochemists typically use a gel medium - usually polyacrylamide, dextran or agarose - and filter under low pressure. Polymer chemists typically use either a silica or cross-linked polystyrene medium under a higher pressure. These media are known as the stationary phase.

The advantage of this method is that the various solutions can be applied without interfering with the filtration process, while preserving the biological activity of the particles to be separated. The technique is generally combined with others that further separate molecules by other characteristics, such as acidity, basicity, charge, and affinity for certain compounds.

The underlying principle of SEC is that particles of different sizes will elute (filter) through a stationary phase at different rates. This results in the separation of a solution of particles based on size. Provided that all the particles are loaded simultaneously or near simultaneously, particles of the same size should elute together.

This is usually achieved with an apparatus called a column, which consists of a hollow tube tightly packed with extremely small porous polymer beads designed to have pores of different sizes. These pores may be depressions on the surface or channels through the bead. As the solution travels down the column some particles enter into the pores. Larger particles cannot enter into as many pores. The larger the particles, the less overall volume to traverse over the length of the column, and the faster the elution.

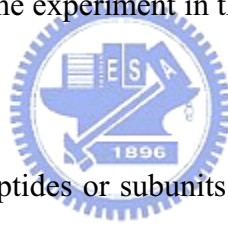
The filtered solution that is collected at the end is known as the eluent. The void volume consists of any particles too large to enter the medium, and the solvent volume is known as the column volume.

Proteins and other biomolecules often differ greatly from each other in their mass and shape. Gel filtration chromatography (also known as molecular sieve or size exclusion chromatography) takes advantage of this difference by retaining biomolecules of a given size range and fractionating them in a manner related to their mass in a form of partition chromatography. This is possible because the stationary phase employed in this method is made up of a gel consisting of beads containing pores of a defined and narrow size range. These will allow only biomolecules below a particular mass to diffuse into the pore. This is referred to as the cutoff value or exclusion limit of the stationary phase. Once inside the bead, the biomolecule will be retained momentarily in channels passing through it. As the sample progresses through a bed of such stationary phase, smaller molecules will be retained more readily than larger ones. Molecules of greater mass than the exclusion limit will pass freely through the column, eluting in a single, unresolved, peak at the void volume. Molecules within the fractionation range of the gel, however, will be retained in a manner generally inversely proportional to their mass, i.e. smaller molecules will be retained longest. The fractionation range and resolution achievable with such a chromatography system will depend greatly on the composition and uniformity of the population of beads in the stationary phase.

Gel filtration chromatography has three main applications in biochemistry. It may be used in a routine way to remove low molecular weight components from samples. For example, it is possible to desalt protein solutions by passage through a column of Sephadex G-25 (fractionation range 1~5kDa). This application takes advantage of the cutoff value of these beads (5kDa) rather than of their fractionation range. Such chromatography is also useful for rapid exchange into a buffer of different composition with minimum dilution of protein sample.

A second application depends on the fact that the elution volume of proteins from gel filtration columns depends on their mass. Thus, if we determine the elution volumes of

proteins of known mass on a given gel filtration column, we can easily determine the mass of a protein of unknown mass by plotting $\log M_r$ versus elution volume. This mass is the native mass of the protein. It is important to note that this experiment makes a number of important assumptions. First, it assumes that the protein has a similar shape to the standards used (i.e. proteins of known mass). This is acceptable if both the protein and standards are globular, for example. However, molecules with large axial ratios (i.e. rod-like in shape rather than globular) such as collagen behave as if they have a much greater mass on gel filtration. Where little is known about the overall shape of the protein, care should be taken in interpreting gel filtration data. A further point to note is that some proteins may experience secondary ionic or ion exchange interactions with the stationary phase beads. This can result in the molecules being retained on gel filtration in a way which may not depend on mass alone. One means of avoiding such effects is to carry out the experiment in the presence of 100~300 mM NaCl or a similar salt.



The mass of individual polypeptides or subunits of which oligomeric proteins are composed may be determined under denaturing conditions by a number of techniques such as SDS polyacrylamide gel electrophoresis or mass spectrometry. Determination of native mass may help us to determine the quaternary structure of proteins by comparison with results from denaturing experiments.

A third application of gel filtration chromatography is in protein purification. Since the method depends on molecular mass, it may be used to separate proteins based on differences in their mass. An important limitation to this approach is the loading volume which can be achieved. Generally, this is a maximum of approximately 5% of the bed volume of the column. This technique is therefore often used near the end of a purification strategy as a polishing step. Neither gel filtration nor ion exchange chromatography alone is capable of achieving complete purification of proteins. However, since it is unlikely that two proteins

will have the same net charge and mass, combining the two approaches can often achieve impressive purification.

2.3.2.4 : Ion Exchange chromatography

Ion-exchange chromatography is a process that allows the separation of ions and polar molecules based on the charge properties of the molecules. It can be used for almost any kind of charged molecule including large proteins, small nucleotides and amino acids, with the experimental solution to be separated collectively known as the analyte. It is often used as a first step in protein purification.

Ion exchange chromatography retains analyte molecules based on coulombic (ionic) interactions. The stationary phase surface displays ionic functional groups that interact with analyte ions of opposite charge. This type of chromatography is further subdivided into cation exchange chromatography and anion exchange chromatography:

1. Cation exchange chromatography retains positively charged cations because the stationary phase displays a negatively charged functional group such as a phosphoric acid.
2. Anion exchange chromatography retains negatively charged anions using positively charged functional group such as a quaternary ammonium cation.

2.3.2.5 : Bioaffinity chromatography

This chromatographic process relies on the property of biologically active substances to form stable, specific, and reversible complexes. The formation of these complexes involves the participation of common molecular forces such as the Van der Waal's interaction,

electrostatic interaction, dipole-dipole interaction, hydrophobic interaction, and the hydrogen bond. An efficient, biospecific bond is formed by a simultaneous and concerted action of several of these forces in the complementary binding sites.

2.3.3 : Scanning Electron Microscopy

The scanning electron microscope (SEM) is a type of electron microscope capable of producing high-resolution images of a sample surface. Due to the manner in which the image is created, SEM images have a characteristic three-dimensional appearance and are useful for judging the surface structure of the sample. The SEM was pioneered by Manfred von Ardenne in the 1930s. The instrument was further developed by Charles Oatley and first commercialized by Cambridge Instruments.

In a typical SEM, electrons are thermionically emitted from a tungsten or lanthanum hexaboride (LaB_6) cathode and are accelerated towards an anode; alternatively, electrons can be emitted via field emission (FE). Tungsten is used because it has the highest melting point and lowest vapour pressure of all metals, thereby allowing it to be heated for electron emission. The electron beam, which typically has an energy ranging from a few hundred eV to 100 keV, is focused by one or two condenser lenses into a beam with a very fine focal spot sized 1 nm to 5 nm. The beam passes through pairs of scanning coils in the objective lens, which deflect the beam horizontally and vertically so that it scans in a raster fashion over a rectangular area of the sample surface. When the primary electron beam interacts with the sample, the electrons lose energy by repeated scattering and absorption within a teardrop-shaped volume of the specimen known as the interaction volume, which extends from less than 100 nm to around 5 μm into the surface. The size of the interaction volume depends on the beam accelerating voltage, the atomic number of the specimen and the specimen's density. The energy exchange between the electron beam and the sample results in the emission of electrons and electromagnetic radiation which can be detected to produce an image, as described below.

2.4 : Experiments

2.4.1 : Find the stable condition for Spidroin from major gland

In order to storage our sample stably. We need to find stable physiological parameters, such as pH and ions etc. We controlled (1) concentration of KCl, (2) pH of the solution, (3) concentration of urea, (4) Storage temperature to find stable zone of spidroin. Concentration of KCl was tested from 100mM to 800mM, pH value from 2.0 to 8.0, concentration of urea from 0M to 4M and storage temperature was controlled at -80°C , 4°C , 37°C . If the testing solution occurred precipitation means that the spidroin was not stable in the buffer.

Preparation of spider major ampullate gland

Mature female *Nephila pilipes* spiders, in which the major glands are very prominent, were collected. The dissected abdominal part of *Nephila pilipes* spider, see Fig. 19. The major ampullate gland from *Nephila pilipes* spider, see Fig. 20.



Fig 19: The abdominal part of the spider.



Fig 20: The major ampullate glands of spider.

2.4.2 : Analysis of Spidroin by SDS-PAGE

Major glands from selected spiders were harvested. Part of the harvested major glands was dissolved in sample buffer for SDS-PAGE analysis.

1. Making 8% separating gel with H₂O 4.68ml, 1.5M Tris-HCl (pH 8.8) 2.5ml, 40% Acrylamide-bis 2.67ml, 10% SDS 100 μ l, 10% APS 50 μ l and TEMED 10 μ l.
2. Making 4% stacking gel with H₂O 3.05ml, 0.5M Tris-HCl (pH 6.8) 1.25ml, 40% Acrylamide-bis 650 μ l, 10% SDS 50 μ l, 10% APS 25 μ l and TEMED 10 μ l.
3. Assembling the gel apparatus and filled with 1 \times running buffer.
4. Mixing protein samples with 5 \times sample buffer containing SDS.
5. Heat the mixture at 95 $^{\circ}$ C for 5min.
6. Loading samples and running the electrophoresis.
7. Staining the separated proteins with Coomassie Blue for 20min.
8. Destained the gel with destain I for 30min.
9. Destained the gel with destain II overnight.



2.4.3 : Analysis of Spidroin by High performance liquid chromatography

The High Performance Liquid Chromatography system consisted of one L-2100 pump, L-2200 Autosampler, and L-2450 diode array detector all from Hitachi (Tokyo, Japan). Separations were performed on a SynChropak GPC 4000 column (250 \times 4.6 mm, Eprogen Inc.). The mobile phase was PBS (pH 7.0) and flow rate was 0.5ml/min.

2.4.4 : Preparation of gold nanoparticles

The seed colloids were prepared by adding 1 mL of 0.25mM HAuCl₄ to 90 mL of H₂O and stirred for 1 min at 25 °C. Two milliliters of 38.8 mM sodium citrate was added to the solution and stirred for 1 min followed by addition of 0.6 mL freshly prepared 0.1 M NaBH₄ in 38.8 mM sodium citrate. Different diameters of gold nanoparticles ranging from 3.5 nm to 12 nm were generated by changing the volume of seed colloid added. The solution was stirred for an additional 5 to 10 min at 0 to 4 °C (Brown, Walter, Natan, 2000, Chem Mater, 12, 306-313). Fifty microliters of 0.1M ascorbic acid, 9mL growth solution (0.25mMHAuCl₄, 0.08M cetyltrimethylamonium bromide), and 1.0mL Seed colloid (8.0±0.8nm in diameter) was combined in a glass beaker, followed by continuous stirring for 10 to 20 min at room temperature until the solution turned reddish brown (approximately 17 nm) or brown (37 nm).

2.4.5 : Self-assembly of spidroin to form protein nanostructure

To self-assembly of spidroin to protein structure, we tried many physiological parameters, such as temperature, incubation time, concentration of spidroin. Finally, we found some condition that can lead spidroin to self-assembly into wanted protein structure.

As to temperature, we tried 25°C, 37°C and 50°C. The results showed that 37°C was the best condition to let spidroin to self-assembly. As for incubation time, we tried 1day to 7days. The results showed one day for self-assembly. As regards to concentration, we finally obtained that 0.5mg/ml is better.

We used Si wafer as substrate to self-assembly spidroin. Before dropping the spidroin, the Si wafer cleaned by SPM procedure. (volume of H₂SO₄ : volume of H₂O₂ = 3 : 1)

After dropping spidroin to cleaned Si wafer, incubated in 37°C for one day. Then, samples were dehydrated (See section 2.4.6) and observed by scanning electron microscopy.

2.4.6 : Self-assembled protein nanostructures with gold nanoparticles

After synthesizing those net-like protein nanostructures. We tried to combine different size gold nanoparticles to these special protein nanostructures. We tried 5nm, 13nm, 17nm, 37nm, 50nm. Only size in 37nm presented obviously composite structures. The SEM image shows the 37nm gold nanoparticles combined with our special net-like protein nano structures. See Fig. 25.

2.4.7 : Organic solvents induced protein structure

The molecular mechanism of spinning process involves the conversion of a highly concentrated, predominantly disordered silk protein (spidroin) into β -sheet-rich structures. So we tried some organic solvents to induced protein converted to β -sheet-rich structures.

We used Si wafer as substrate to self-assemble spidroin. Before dropping the mixture, the Si wafer cleaned by SPM procedure. (volume of H_2SO_4 : volume of H_2O_2 = 3 : 1) After dropping mixture to cleaned Si wafer, incubated at $37^\circ C$ for one day. Then, samples were dehydrated (See section 2.4.6) and observed by scanning electron microscopy.

We tried three kinds of organic solvents to induced protein structure, methanol, ethanol and isopropyl alcohol. The results showed different level of induced structures formation. As the concentration of organic solvents increased the more obvious induced structures formed.

2.4.8 : Scanning electron microscopy of Self-assembled protein nanostructure

For SEM were fixed with 1.25% glutaraldehyde (contained 2% tannic acid) in PBS buffer for 1 hr. Postfixation with 6.25% osmium tetroxide solution in PBS for 30 min, then the sample were dehydrated in ethanol from 50% to absolute ethanol. Finally, added HMDS for drying overnight.[47]

SEM: Fixation and dehydrate process

1. Fixed sample with 1.25% glutaraldehyde (contained 2% tannic acid) for 1hr.
2. Rinsed with DI water for 5min, three time.
3. Postfixed sample with 6.25% osmium tetroxide for 30min.
4. Rinsed with DI water for 5min, three times.
5. Sample were dehydrated with 50% ethanol for 5min.
6. Sample were dehydrated with 60% ethanol for 5min.
7. Sample were dehydrated with 70% ethanol for 5min.
8. Sample were dehydrated with 80% ethanol for 5min.
9. Sample were dehydrated with 90% ethanol for 5min.
10. Sample were dehydrated with 95% ethanol for 5min, two times.
11. Sample were dehydrated with absolute ethanol for 5min, three times.
12. 100%HMDS dried overnight.

All samples were pulse sputter-coated with platinum JEOL JFC-1600 Auto Fine Coater and then examined with a JEOL SEM-6700F scanning electron microscope (JEOL USA, Peabody, Massachusetts, USA) equipped with a lanthanum hexaboride (LaB₆) gun at 10 kV.

Chapter 3 : Results and Discussion

3.1 : Stable condition for spidroin from major gland

We controlled (1) concentration of KCl, (2) pH of the solution, (3) concentration of urea, (4) Storage temperature to find stable zone of spidroin. Concentration of KCl tested from 100mM to 800mM, pH value from 2.0 to 8.0, concentration of urea from 0M to 4M and storage temperature was controlled at -80°C , 4°C , 37°C . If the testing solution occurred precipitation means that the spidroin was not stable in the buffer. (see Fig. 21)

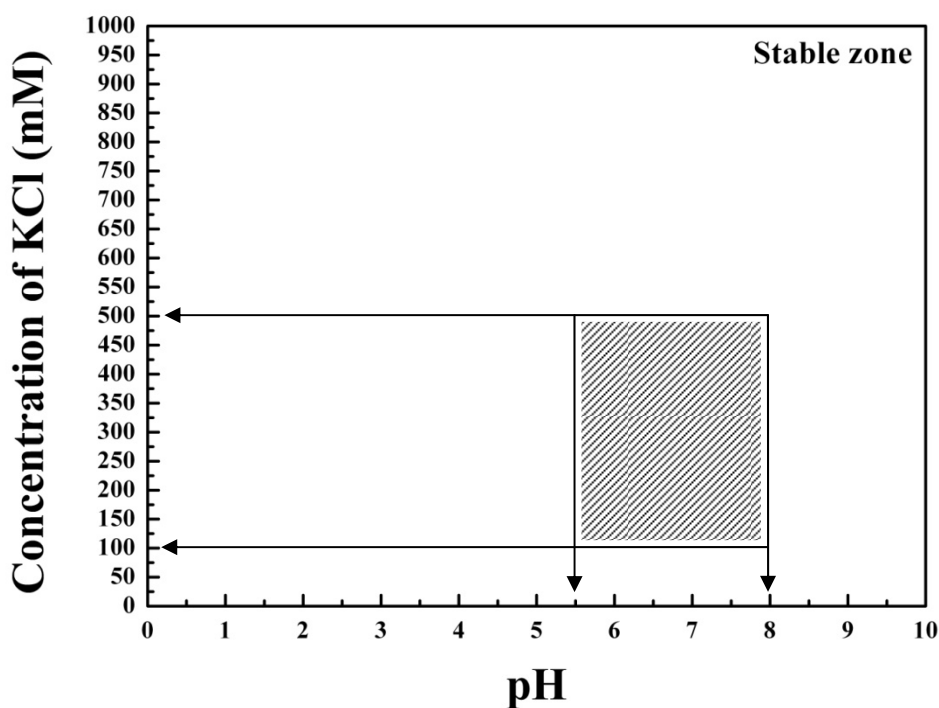


Fig 21: The phase diagram of spidroin.
Phase diagram shows the stable zone of spidroin.

3.2 : SDS-PAGE analysis of spidroin

The major ampullate gland proteins analyzed by SDS-PAGE electrophoresis. Our spidroin molecular weight were mainly 70kDa and some little molecular proteins else. (see Fig. 22)

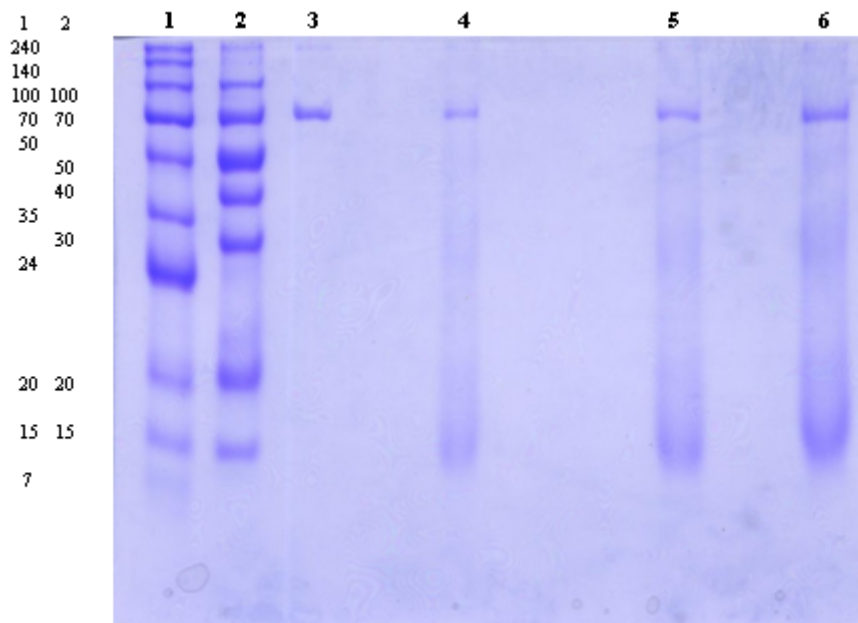


Fig 22: SDS-PAGE electrophoresis of spidroin.

Lane 1: Broad-range marker, Lane 2: Middle-range marker, Lane 3: BSA 0.1mg/ml, Lane 4: Spidroin 0.5mg/ml 10µl, Lane 5: Spidroin 0.5mg/ml 15µl, Lane 6: Spidroin 0.5mg/ml 20µl.

3.3 : High performance liquid chromatography analysis of spidroin

We also analyzed spidroin with gel-filtration HPLC. The results showed that also had molecular weight about 70kDa. Results presented spidroin were pure with single sharp peak. Retention time were 6.5min for 0.5ml/min flow rate and the mobile phase were used PBS (pH 7.0). Different injection volume were showed in the Fig. 23.

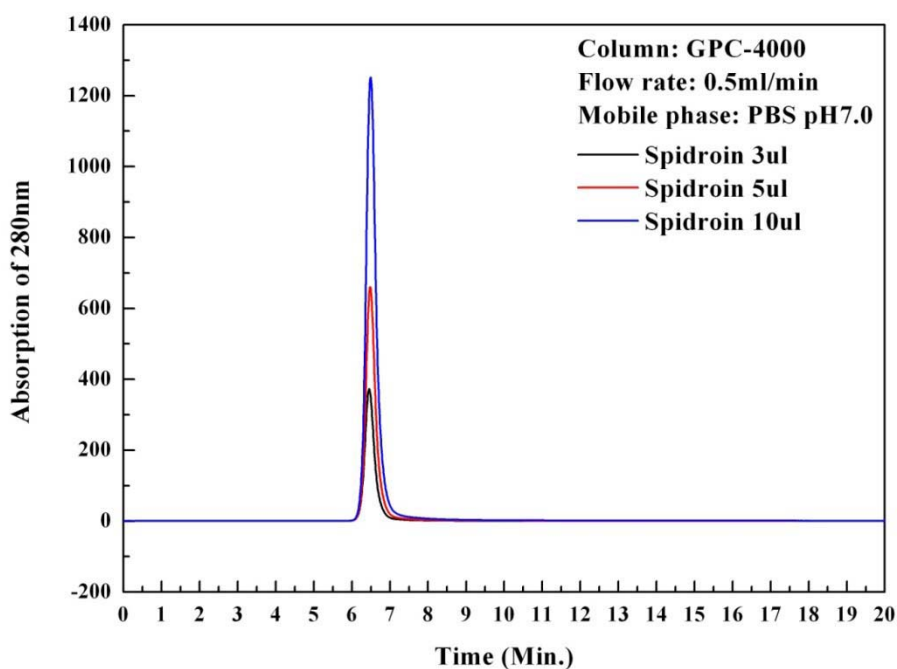


Fig 23: Gel-filtration of spidroin.

Gel-filtration column presented single sharp peak, and eluted at about 6.5 min. The molecular weight was almost the same with BSA. So the molecular weight was about 70kDa.

3.4 : Self-assembled protein nanostructures

We used Si wafer as substrate to self-assemble spidroin. Before dropping the spidroin, the Si wafer cleaned by SPM procedure. (volume of H_2SO_4 : volume of H_2O_2 = 3 : 1) After dropping spidroin to cleaned Si wafer, incubated in 37°C for one day. Then, samples were dehydrated (See section 2.4.6) and observed by scanning electron microscopy. The SEM images showed net-like nano protein structures. (see Fig. 24)

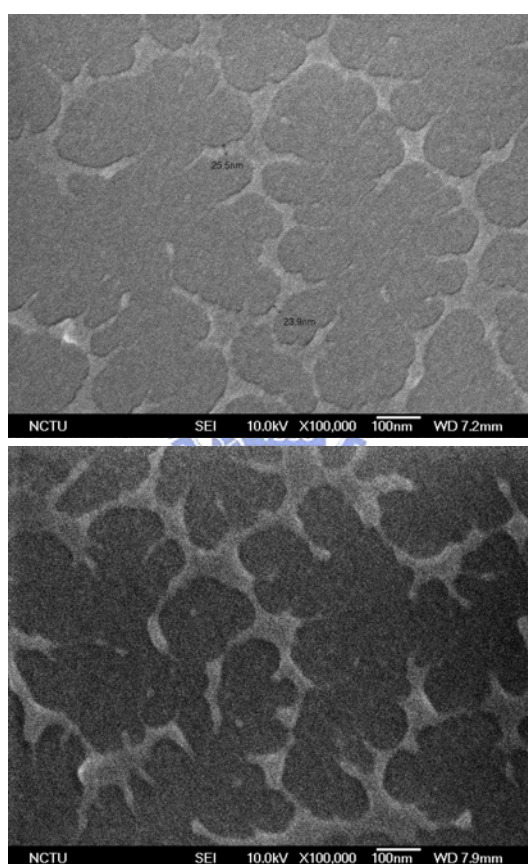


Fig 24: SEM images of self-assemble protein nano structures.

3.5 : Self-assembled protein nanostructures combined with gold nanoparticles

In section 3.4, we synthesized net-like protein nanostructures. We tried to combine gold nanoparticles to these special protein nanostructures. The SEM image shows the gold nanoparticles combined with our special net-like protein nanostructures. The size of gold nanoparticles combined with our special net-like protein nanostructures. The size of gold nanoparticles were 37nm. See Fig. 25.

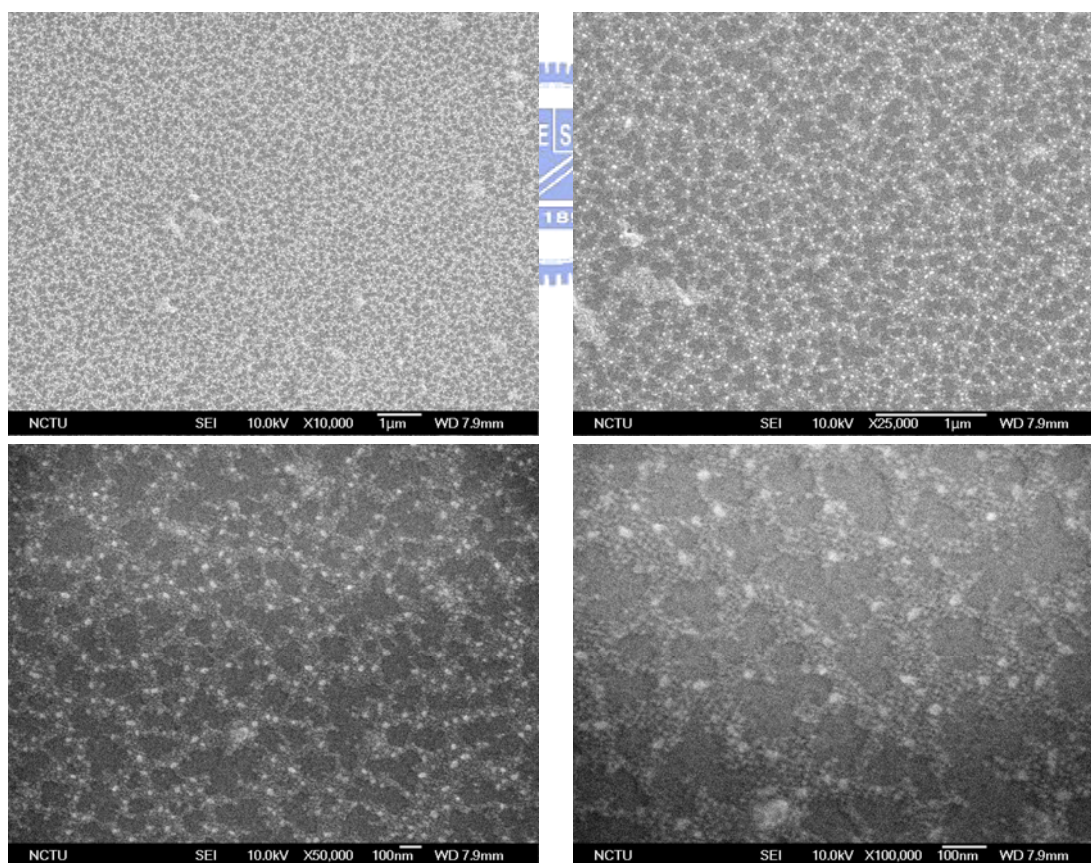


Fig 25: SEM images of self-assemble protein nano structures with 37nm gold nanoparticles.

3.6 : Organic solvents induced protein structures

How does alcohol induce the secondary structure transition in spidroin?

There are three direct effects. It can summarize the generally agreed mechanism of the alcohol-induced conformational change in globular proteins: (1) local interactions (strengthening of intramolecular H-bonds), (2) non-local interactions (weakening of hydrophobic interactions) and (3) preferential solvation. Practically, the addition of alcohol will decrease solvent polarity hence weaken the hydrophobic interactions that stabilize the native structure. Alternatively, the protein-protein interactions are weakened and simultaneously the local hydrogen bonds are strengthened, resulting in denaturation or dissolution and stabilization of the extended helical structures [48, 49].

Relatively unknown is the behavior of natively unfolded proteins in water/organic mixtures [50]. Munishkina et al. [51] observed that structural transformation and oligomerization of the intrinsically disordered α -synuclein depended on the alcohol nature and especially their concentration. They concluded that β -sheet structure formation of α -synuclein in presence of simple alcohols (MeOH, EtOH, IsoP) or low concentration of TFE was due solely to the decrease in dielectric constant. In contrast, α -helical structure formation in the presence of fluorinated alcohols could be assigned to preferentially binding of the alcohol to the proteins in addition to decrease in dielectric constant.

MeOH, EtOH and IsoP induced a coil to β -sheet type transition in spidroin. Ishida et al. [52] used NMR to monitor the effects of various organic solvent on regenerated silkworm fibroin membrane and showed that hydration induces a conformational readjustment of the random coil structure to a Silk I type or partial conversion to β -sheet rich structure (Silk II) depending on the hydrophilic site and stability of the alanine helical domains. The former behavior was observed with *B. mori*, and the latter with the less stable *Philosamia Cynthia ricini* fibroin conformation of this spidroin I-like protein (T. Asakura personal

communication). Ishida et al. [52] also showed that highly miscible organic solvents are more likely to induce a change of conformation to the β -sheet rich state (Silk II) with the diffusion of the solvent into the protein being the rate-limiting step. They noted that in solution the conformational change induced by the organic solvent was faster in the following series: methanol > ethanol > propanol > pyridine > acetone > pentanol > butanol > chloroform.

Cedric Dicko et, al. shows formation of helices upon addition of TFE and HFIP is most likely dominated by a decrease in solvent dielectric constant enhanced by preferential solvation of the protein by the fluorinated alcohol [53]. The formation of the β -sheet structure with simple alkyl alcohols although consistent with the observed behavior of intrinsically disordered protein shows an inverse dependence of kinetics of oligomerization/aggregation with decrease dielectric constant. MeOH, high dielectric constant, gives the fastest kinetics of conversion. This suggests that simple alcohol might also preferentially solvate spidroin or that the miscibility of the alcohol is the limiting factor to the kinetic. We should nevertheless keep in mind other parameters not considered here might also be crucial, for example, protein dispersity, pH, concentration, exposed hydrophobic residues and overall physiological condition of the spider [54].

3.6.1 : Methanol treatment with spidroin

We mixed spidroin with gradient methanol concentration to induce protein structures. Methanol concentration was from 0% to 80%. The samples were reacted with methanol for 30min. Then, 10 μ l of mixture was dropped to Si wafer. Samples were incubated at 37 $^{\circ}$ C for one day. Results show in the Fig. 25. We can observe that as the concentration of methanol increase, the disordered silk structure become contracting to net-like structure.

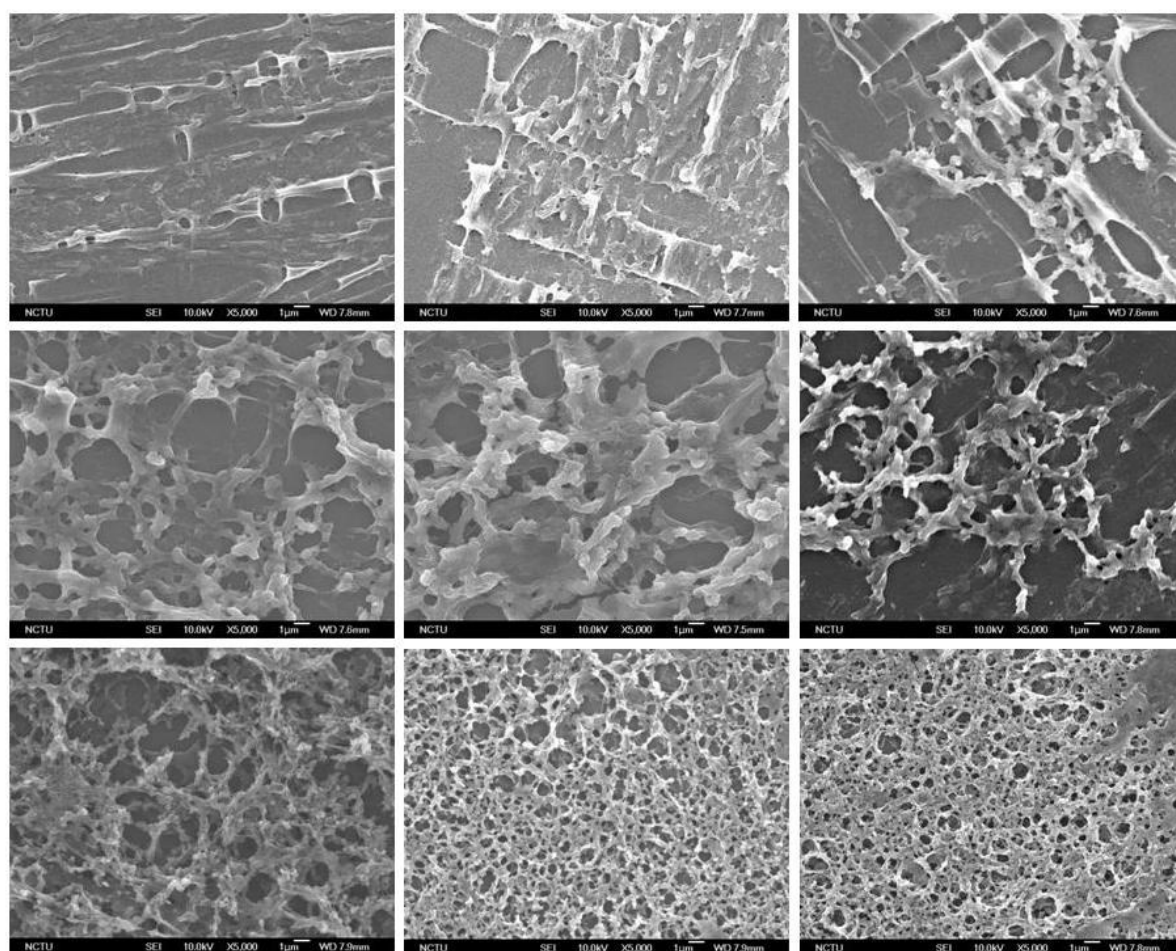


Fig 26: SEM images of methanol induced protein structures.

SEM images showed isopropyl alcohol induced protein net structures. Top row 0%~20% methanol from left to right, middle row 30%~50% methanol from left to right, bottom row 60%~80% methanol from left to right.

3.6.2 : Ethanol treatment with spidroin

We mixed spidroin with gradient ethanol concentration to induce protein structures. Ethanol concentration was from 0% to 80%. The samples were reacted with ethanol for 30min. Then, 10 μ l of mixture was dropped to Si wafer. Samples were incubated at 37 $^{\circ}$ C for one day. Results show in the Fig. 26.

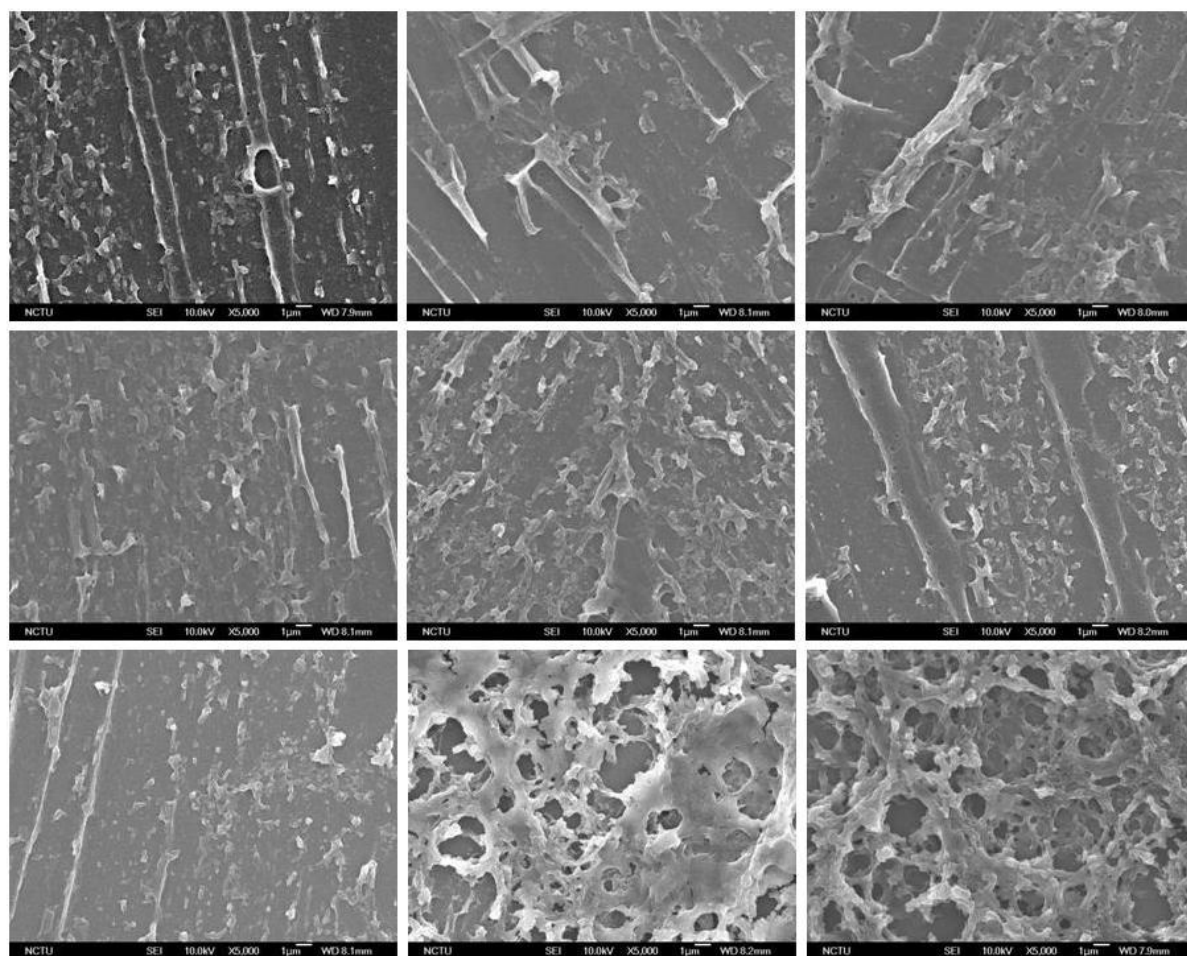


Fig 27: SEM images of ethanol induced protein structures.

SEM images showed isopropyl alcohol induced protein net structures. Top row 0%~20% ethanol from left to right, middle row 30%~50% ethanol from left to right, bottom row 60%~80% ethanol from left to right.

3.6.3 : Isopropyl alcohol treatment with spidroin

We mixed spidroin with gradient isopropyl alcohol concentration to induce protein structures. Isopropyl alcohol concentration was from 0% to 80%. The samples were reacted with isopropyl alcohol for 30min. Then, 10 μ l of mixture was dropped to Si wafer. Samples were incubated at 37 $^{\circ}$ C for one day. Results show in the Fig. 27.

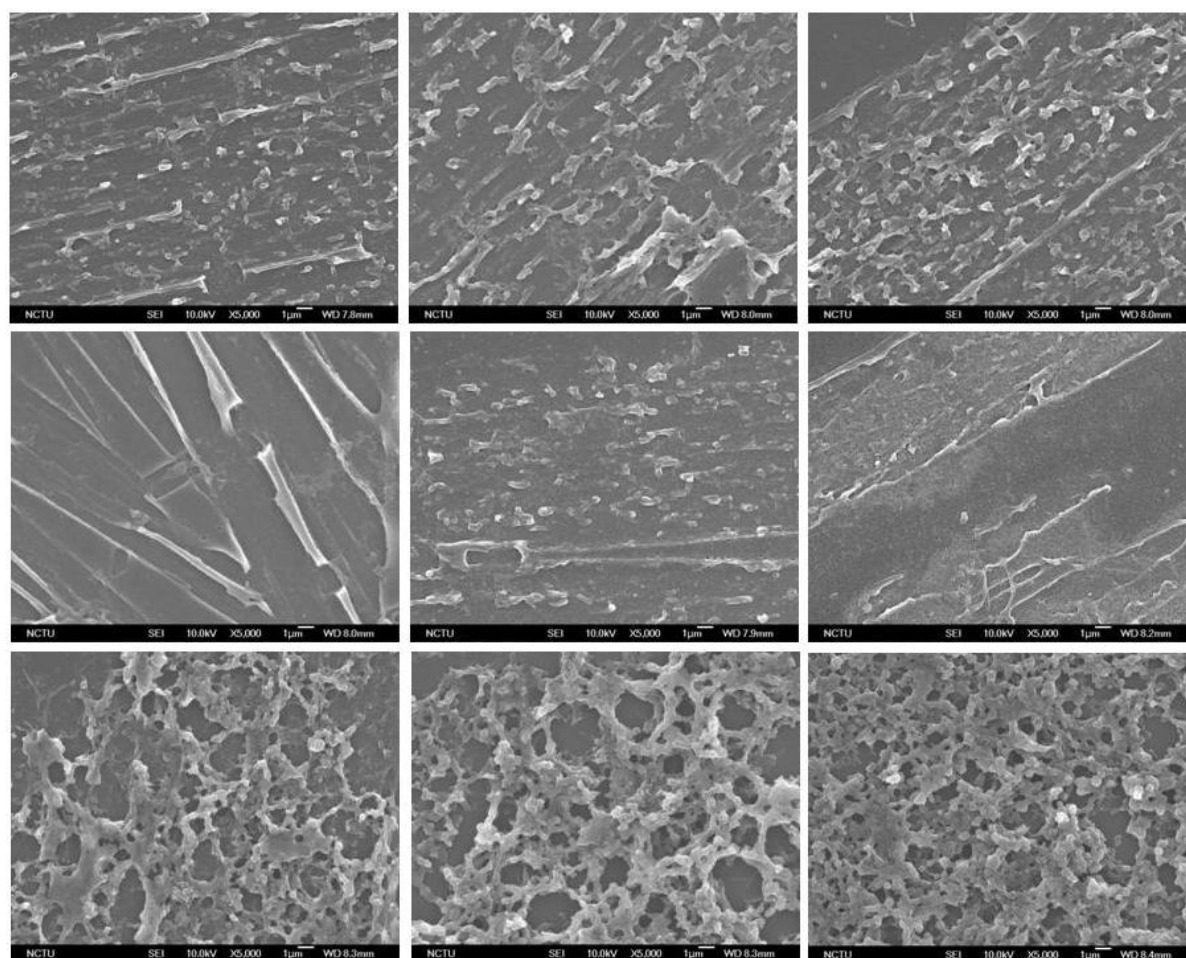


Fig 28: SEM images of isopropyl alcohol induced protein structures.

SEM images showed isopropyl alcohol induced protein net structures. Top row 0%~20% isopropyl alcohol from left to right, middle row 30%~50% isopropyl alcohol from left to right, bottom row 60%~80% isopropyl alcohol from left to right.

3.7 : Summary

We found the stable condition to storage spidroin successfully, and tried some condition to self-assemble the spidroin. We successfully applied spidroin to self-assemble into net-like protein nanostructures. We also wanted to application of these net-like protein nanostructures to form composite materials. We used biocompatible gold nanoparticles to combine with our special net-like protein nanostructures successfully. In section 3.5, results show the special composite materials.

Refer to organic solvents induced structures, we found that methanol had best structures at high concentration. Ethanol and isopropyl alcohol also induced structure formation.

Chapter 4 : Conclusion



First, we found the stable buffer to storage spidroin. Because of urea, spidroin was at denatured state. It means that spidroin lost their original functions. But we tried a lot of conditions to let spidroin to self-assemble into silk-like or net-like structures.

Second, we successfully used natural spidroin to self-assembled protein structure. There are many researches about spidroin. Refer to self-assembled structures. Most study use regenerated peptides to self-assemble. There are no any other researches mentioned directly use natural spidroin to form any structures.

Third, we used three organic solvents, methanol, ethanol, isopropyl alcohol to promote spidroin self-assembled structures formation. The structures have silk-like and net-like structure.

Chapter 5 : Future perspective

There are many researches about spider silk. No previous studies mentioned directly apply natural spidroin to assemble protein nanostructures.

We tried out some conditions to self-assembled natural spidroin, and formed some special structures successfully. In future, first, we need to measure the basic characteristics of these protein structures. Second, we will focus on application of these structures to combine with inorganic materials – gold nanoparticles. We hope that our composite material could have some special characteristics. The composite material might have different properties from natural spider silk. It might have strong mechanical properties from spidroin and conductivity from gold nanoparticles. If we have ability to control these self-assembled structures of spidroin. These protein structures will have a lot of applications.



Chapter 6 : References

1. Lewis, M.X.a.R.V., *Structure of a Protein Superfiber: Spider Dragline Silk*. Proc. Natl. Acad. Sci. USA, 1990. **87**: p. 7120.
2. Vollrath, F., *Strength and structure of spiders' silks*. Reviews in Molecular Biotechnology, 2000. **74**: p. 67.
3. Editorial, *Silk biotechnology*. Reviews in Molecular Biotechnology, 2000. **74**: p. 65.
4. Michael B. Hinman, J.A.J.a.R.V.L., *Synthetic spider silk: a modular fiber*. TIBTECH, 2000. **18**: p. 374.
5. Todd A. Blackledge, a.C.Y.H., *Silken toolkits: biomechanics of silk fibers spun by the orb web spider *Argiope argentata* (Fabricius 1775)*. The Journal of Experimental Biology, 2006. **209**: p. 2452.
6. J. M. GOSLINE, P.A.G., C. S. ORTLEPP AND K. N. SAVAGE, *THE MECHANICAL DESIGN OF SPIDER SILKS: FROM FIBROIN SEQUENCE TO MECHANICAL FUNCTION*. The Journal of Experimental Biology, 1999. **202**: p. 3295.
7. Ning Du, X.Y.L., Janaky Narayanan, Lian Li, Matthew Lek Min Lim,y and Daiqin Liy, *Design of Superior Spider Silk From Nanostructure to Mechanical Properties*. Biophysical Journal, 2006. **91**: p. 4528.
8. Stefan Winkler, D.L.K., *Molecular biology of spider silk*. Reviews in Molecular

- Biotechnology, 2000. **74**: p. 85.
9. Alexander Spönnner, B.S., Fritz Vollrath, Eberhard Unger, Frank Grosse, and Klaus Weisshart, *Characterization of the Protein Components of Nephila clavipes Dragline Silk*. Biochemistry, 2005. **44**: p. 4727.
 10. Barbara A. Lawrence, C.A.V., and Anne M. F. Moore, *Molecular and Mechanical Properties of Major Ampullate Silk of the Black Widow Spider, Latrodectus hesperus*. Biomacromolecules, 2004. **5**: p. 689.
 11. ALEXANDER SPÖNNNER, E.U., FRANK GROSSE AND KLAUS WEISSHART, *Differential polymerization of the two main protein components of dragline silk during fiber spinning*. Nature materials, 2005. **4**: p. 772.
 12. Amanda E. Brooks, H.B.S., Shane R. Nelson, and Randolph V. Lewis, *An Investigation of the Divergence of Major Ampullate Silk Fibers from Nephila clavipes and Argiope aurantia*. Biomacromolecules, 2005. **6**: p. 3095.
 13. I-Min Tso, H.-C.W.a.I.-R.H., *Giant wood spider Nephila pilipes alters silk protein in response to prey variation*. The Journal of Experimental Biology, 2005. **208**: p. 1053.
 14. Bo Madsen, Z.Z.S., Fritz Vollrath, *Variability in the mechanical properties of spider silks on three levels: interspecific, intraspecific and intraindividual*. International Journal of Biological Macromolecules, 1999. **24**: p. 301.
 15. Catherine L. Craig, C.R., Marie E. Herberstein, Robert S. Weber, David Kaplan, and Naomi E. Pierce, *Evidence for Diet Effects on the Composition of Silk Proteins Produced by Spiders*. Mol. Biol. Evol., 2000. **17**: p. 1904.
 16. John Gatesy, C.H., Dagmara Motriuk, Justin Woods, Randolph Lewis *Extreme diversity, conservation, and convergence of spider silk fibroin sequences*. SCIENCE, 2001. **291**: p. 2603.
 17. Kaplan, H.-J.J.D.L., *Mechanism of silk processing in insects and spiders*. Nature, 2003. **424**: p. 1057.
 18. Daniel Huemmerich, C.W.H., Susanne Quedzuweit, Jan Oschmann, Rainer Rudolph, and Thomas Scheibel, *Primary structure elements of spider dragline silks and their contribution to protein solubility*. Biochemistry, 2004. **43**: p. 13604.
 19. Anthoula Lazaris, S.A., Yue Huang, Jiang-Feng Zhou, Francois Duguay, Nathalie Chretien, Elizabeth A. Welsh, Jason W. Soares, Costas N. Karatzas, *Spider Silk Fibers Spun from Soluble Recombinant Silk Produced in Mammalian Cells*. Science, 2002. **295**: p. 472.
 20. Daniel Huemmerich, T.S., Fritz Vollrath, Shulamit Cohen, Uri Gat, and Shmulik Ittah, *Novel Assembly Properties of Recombinant Spider Dragline Silk Proteins*. Current Biology, 2004. **14**: p. 2070.
 21. Lewis, M.A.C.a.R.V., *Spider minor ampullate silk proteins contain new repetitive sequences and highly conserved non-silk-like "spacer regions"*. Protein Science, 1998. **7**: p. 667.

22. Cedric Dicko, D.K., John M. Kenney, and Fritz Vollrath, *Secondary Structures and Conformational Changes in Flagelliform, Cylindrical, Major, and Minor Ampullate Silk Proteins. Temperature and Concentration Effects*. *Biomacromolecules*, 2004. **5**: p. 2015.
23. Oskar Liivak, A.F., Randolph Lewis, and Lynn W. Jelinski, *Conformation of the Polyalanine Repeats in Minor Ampullate Gland Silk of the Spider *Nephila clavipes**. *Macromolecules*, 1997. **30**: p. 7127.
24. Cheryl Y. Hayashi, N.H.S., Randolph V. Lewis, *Hypotheses that correlate the sequence, structure, and mechanical properties of spider silk proteins*. *International Journal of Biological Macromolecules*, 1999. **24**: p. 271.
25. Lewis, C.Y.H.a.R.V., *Evidence from flagelliform silk cDNA for the structural basis of elasticity and modular nature of spider silks*. *J. Mol. Biol.*, 1998. **275**: p. 773.
26. Zschokke, S.P.B.a.S., *Untangling the Tangle-Web: Web Construction Behavior of the Comb-Footed Spider *Steatoda triangulosa* and Comments on Phylogenetic Implications (Araneae: Theridiidae)*. *Journal of Insect Behavior*, 2002. **15**: p. 791.
27. Cheryl Y. Hayashi, T.A.B., and Randolph V. Lewis, *Molecular and Mechanical Characterization of Aciniform Silk: Uniformity of Iterated Sequence Modules in a Novel Member of the Spider Silk Fibroin Gene Family*. *Molecular Biology and Evolution*, 2004. **21**: p. 1950.
28. Xiaoyi Hu, K.K., Arnold M. Falick, Anne M. F. Moore, Patrick R. Jones, O. David Sparkman, and Craig Vierra, *Egg Case Protein-1 A NEW CLASS OF SILK PROTEINS WITH FIBROIN-LIKE PROPERTIES FROM THE SPIDER LATRODECTUS HESPERUS*. *THE JOURNAL OF BIOLOGICAL CHEMISTRY*, 2005. **280**: p. 21220.
29. Emilia Bramantia, D.C., Claudia Fortea, Mario Giovanneschic, Massimo Masettic, Carlo Alberto Veracinib, *Solid state ¹³C NMR and FT-IR spectroscopy of the cocoon silk of two common spiders* *Spectrochimica Acta Part A*, 2005. **62**: p. 105.
30. Xiaoyi Hu, B.L., Kristin Kohler, Arnold M. Falick, Anne M. F. Moore, Erin McMullen, Patrick R. Jones, and Craig Vierra, *Araneoid Egg Case Silk: A Fibroin with Novel Ensemble Repeat Units from the Black Widow Spider, *Latrodectus hesperus**. *Biochemistry*, 2005. **44**: p. 10020.
31. Aichun Zhao, T.Z., Yanghu SiMa, Yuansong Zhang, Koichi Nakagaki, Yungen Miao, Kunihiro Shiomi, Zenta Kajiura, Yoko Nagata and Masao Nakagaki, *Unique Molecular Architecture of Egg Case Silk Protein in a Spider, *Nephila clavata**. *J. Biochem.*, 2005. **138**: p. 593.
32. Merri Lynn Casem, D.T., Kelly Houchin, *Protein and amino acid composition of silks from the cob weaver, *Latrodectus hesperus* (black widow)*. *International Journal of Biological Macromolecules*, 1999. **24**: p. 103.
33. Xiaoyi Hu, K.K., Arnold M. Falick, Anne M. F. Moore, Patrick R. Jones, and Craig Vierra, *Spider Egg Case Core Fibers: Trimeric Complexes Assembled from TuSp1*,

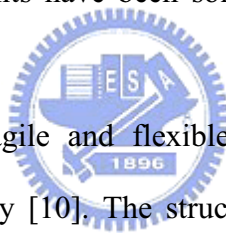
- ECP-1, and ECP-2*. *Biochemistry*, 2006. **45**: p. 3506.
34. Knight, F.V.D.P., *Liquid crystalline spinning of spider silk*. *Nature*, 2001. **410**: p. 541.
 35. Vollrath, F., *Biology of spider silk*. *International Journal of Biological Macromolecules*, 1999. **24**: p. 81.
 36. P. Jeanene Willcox, S.P.G., Wayne Muller and David L. Kaplan, *Evidence of a Cholesteric Liquid Crystalline Phase in Natural Silk Spinning Processes*. *Macromolecules*, 1996. **29**: p. 5106.
 37. Cedric Dicko, F.V., and John M. Kenney, *Spider Silk Protein Refolding Is Controlled by Changing pH*. *Biomacromolecules*, 2004. **5**: p. 704.
 38. F. Vollrath, D.P.K., *Structure and function of the silk production pathway in the Spider Nephila edulis*. *International Journal of Biological Macromolecules*, 1999. **24**: p. 243.
 39. Chuncai Zhou, B.L., Jinrong Yao, Jie Qian, Xin Chen, Ping Zhou, David P. Knight, and Zhengzhong Shao, *Synthesis and Characterization of Multiblock Copolymers Based on Spider Dragline Silk Proteins*. *Biomacromolecules*, 2006. **7**: p. 2415.
 40. Ramin Djalali, Y.-f.C., and Hiroshi Matsui, *Au Nanowire Fabrication from Sequenced Histidine-Rich Peptide*. *J. AM. CHEM. SOC.*, 2002. **124**: p. 13660.
 41. Ramin Djalali, J.S., and Hiroshi Matsui, *Doughnut-Shaped Peptide Nano-Assemblies and Their Applications as Nanoreactors*. *J. AM. CHEM. SOC.*, 2004. **126**: p. 7935.
 42. Mudalige Thilak Kumara, N.S., Subra Muralidharan, and Brian C. Tripp, *Bioengineered Flagella Protein Nanotubes with Cysteine Loops: Self-Assembly and Manipulation in an Optical Trap*. *Nano Lett.*, 2006. **6**: p. 2121.
 43. Ohad Carny, D.E.S., and Ehud Gazit, *Fabrication of Coaxial Metal Nanocables Using a Self-Assembled Peptide Nanotube Scaffold*. *Nano Lett.*, 2006. **6**: p. 1594.
 44. Sogah, O.R.a.D.Y., *Self-Assembly of beta-Sheets into Nanostructures by Poly(alanine) Segments Incorporated in Multiblock Copolymers Inspired by Spider Silk*. *J. Am. Chem. Soc.*, 2001. **123**: p. 5231.
 45. Amit Singh, S.H., and Murali Sastry, *Spider Silk as an Active Scaffold in the Assembly of Gold Nanoparticles and Application of the Gold-Silk Bioconjugate in Vapor Sensing*. *Small*, 2007. **3**: p. 466.
 46. Katharina Janek, J.B., Josef Zipper, Heinz Fabian, Yannis Georgalis, Michael Beyermann, Michael Bienert, and Eberhard Krause, *Water-Soluble beta-Sheet Models Which Self-Assemble into Fibrillar Structures*. *Biochemistry*, 1999. **38**: p. 8246.
 47. F. Braet, R.D.Z.a.E.W., *Drying cells for SEM, AFM and TEM by hexamethyldisilazane: a study on hepatic endothelial cells*. *Journal of microscopy*, 1997. **186**: p. 84.
 48. Bolen, Y.L.a.D.W., *The Peptide Backbone Plays a Dominant Role in Protein Stabilization by Naturally Occurring Osmolytes*. *Biochemistry*, 1995. **34**: p. 12884.
 49. Nami Hirota, K.M.a.Y.G., *Group Additive Contributions to the Alcohol-induced alpha-Helix Formation of Melittin: Implication for the Mechanism of the Alcohol Effects on Proteins*. *J. Mol. Biol.*, 1998. **275**: p. 365.

50. KARIN DAHLMAN-WRIGHT, H.B., IAIN J. MCEWAN, TOVA ALMLÖF, ANTHONY P. H. WRIGHT, and A.T.H. JAN-AKE GUSTAFSSON, *Structural characterization of a minimal functional transactivation domain from the human glucocorticoid receptor*. Proc. Natl. Acad. Sci. USA, 1995. **92**: p. 1699.
51. Larissa A. Munishkina, C.P., Vladimir N. Uversky, and Anthony L. Fink, *Conformational Behavior and Aggregation of alpha-Synuclein in Organic Solvents: Modeling the Effects of Membranes*. Biochemistry, 2003. **42**: p. 2720.
52. Mika Ishida, T.A., Motoko Yokoi, and Hazime Saiti, *Solvent- and Mechanical-Treatment-Induced Conformational Transition of Silk Fibroins Studied by High-Resolution Solid-state ¹³C NMR Spectroscopy*. Macromolecules, 1990. **23**: p. 88.
53. Cedric Dicko, D.K., John M. Kenney, Fritz Vollrath, *Conformational polymorphism, stability and aggregation in spider dragline silks proteins*. International Journal of Biological Macromolecules, 2005. **36**: p. 215.
54. F.N. Braun , C.V., *Modelling self assembly of natural silk solutions*. International Journal of Biological Macromolecules, 2003. **32**: p. 59.



Chapter 1 : Introduction

Ribosomes are the most ubiquitous enzyme performing the most fundamental biochemical reactions in all living organisms, reactions that translate genetic code from messenger RNA and synthesize proteins from amino acyl-transfer RNAs [1, 2]. Ribosomes are composed of two unequally sized subunits with a total molecular weight of about 2,450 kDa. RNA components occupy approximately two-thirds of the mass, while proteins constitute rest of the ribosomes. Prokaryotic ribosomes are characterized by their sedimentation coefficient of 70S, with the large subunit of 50S and small subunit of 30S. To unravel structural basis for the fundamental biological process crystal structures for ribosomes or subunits have been solved in prokaryotes and eukaryotes [3-9].



Ribosomes are structurally fragile and flexible thus tend to deteriorate causing multi-conformational heterogeneity [10]. The structure is also delicately balanced by magnesium ions [11-15]. The absence of magnesium ions causes irreversible change of conformation for 50S subunit. However, there is lack of proper tool to obtain dynamic change of structure.

The flexible and fragile nature of ribosomes complicated the purification and preservation process and presents a challenging task for biochemists. Ultra-centrifugation protocols are applied in majority for the extraction and purification of ribosome [16-19]. The long and tedious protocol takes days to obtain purified ribosome for further application. It is very likely but yet to be proven that the RNA components of ribosome are at risk of partially degradation which causes heterogeneous behaviors. Additionally, the quality of traditionally purified ribosome is less than ideal ($OD_{260/280}$ ratio usually less than 2.0), which is possibly caused by the minor

contamination of small molecules. A rapid and chromatographic method might be of particular interest to overcome these problems. Because the dimension of native 70S ribosome is approximately 20 nm, it is possible to purify ribosome by gel filtration chromatography with sufficiently large pore size.

Methods in chromatographic separation have been applied to purify ribosomes. Hydrophobic interaction chromatography on Sepharose 4B has been used to separate prokaryotic ribosomal subunits [20]. It offers a rapid method for purifying ribosomes away from contaminating nucleases and proteases in the crude preparation. Preparative agarose/acrylamide gel electrophoresis was also applied to obtain high quality ribosomes from crude prep [21]. HPLC equipped with affinity column is also applied to purify yeast ribosomes [22]. Fast exclusion of ribosomes using gel filtration with pore size smaller than ribosomal particles is also demonstrated. However, application of gel-filtration to purify ribosomes from cell extract is yet to be demonstrated. Advantage of gel filtration includes speed, purity, and minor perturbation of the native structure.

Magnesium maintains the native conformation but promote nuclease activity which causes degradation for the RNA component in ribosome. Thus the key issue of ribosome purification is speed. The current study provides a fast and convenient method to isolate ribosome with greater purity. Additionally, gel-filtration-HPLC also provide a convenient and fast analysis of the structural characterization for ribosomes.

*Sedimentation coefficient (S): The sedimentation coefficient of a particle or macromolecule is computed through dividing the constant speed of sedimentation (in ms^{-1}) by the acceleration applied (in ms^{-2}). The speed is constant because the force applied by the ultracentrifuge (measuring typically in multiples of hundreds of thousands of gravities) is canceled by the viscous resistance of the medium (normally water) through which the particle is moving. The result has the dimensions of a unit of time and is expressed in svedbergs. One svedberg is defined as exactly 10^{-13}s .

Bigger particles have higher svedberg values. The svedberg is not additive, since the sedimentation rate is associated with the size of the particle, when two particles bind together there is inevitably a loss of surface area. Thus when measured separately they will have svedberg values that do not add up to that of the particle formed when they bind together.

This is particularly the case with the ribosome. The most important measure used to distinguish ribosomes, which indicates their source organism, is the svedberg. A 70S ribosome comes from eubacteria, but is composed of a 50S subunit and a 30S subunit.

Chapter 2 : Paper Review

2.1 : Introduction of Prokaryotic Ribosome

The ribosome is a large ribo-nucleoprotein particle which consists of two unequal subunits. Prokaryotic ribosomes have a relative sedimentation rate of 70S and can be separated into a large 50S subunit and a small 30S subunit. The 50S subunit contains a 5S (120 nucleotides) and a 23S ribosomal RNA (rRNA) (about 2900 nucleotides), and the 30S subunit contains a single 16S rRNA (approximately 1500 nucleotides). The protein fraction consists of 21 different proteins in the 30S subunit and 33 proteins in the 50S subunit. It is responsible for the translation process in every living cell.

2.2 : Conventional Ultra-Centrifugal Purification of Prokaryotic Ribosome



The conventional purification approaches might take a lot of time. Let us take some example of other purification approaches.

Example 1: Ribosomes were prepared from *E. coli* MRE600 cells. Cells were disrupted by grinding with aluminum oxide in 20 mM tris(hydroxymethyl)aminomethane hydrochloride (Tris-HCl), pH 7.2, 10 mM MgCl₂, 60 mM NH₄Cl, and 10 mM 2-mercaptoethanol. DNase I was added to a final concentration of 5 µg/mL. After the aluminum oxide and cell debris were removed by centrifugation, the supernatant was centrifuged for 90 min at 15 000 rpm (SS34 Sorvall rotor). The supernatant was layered on top of a sucrose cushion (1.1 M sucrose in 50 mM Tris-HCl, pH 7.5, 10 mM MgCl₂, 0.5 M NH₄Cl, and 10 mM 2-mercaptoethanol)

and centrifuged at 38 000 rpm for 24 h (45 Ti rotor). The pellets with the ribosomes were dissolved in 20 mM Tris-HCl, pH 7.5, 6.3 mM MgCl₂, 0.3 mM ethylenediaminetetraacetic acid (EDTA), 100 mM NH₄Cl, and 10 mM 2-mercaptoethanol. 70s tight-couple ribosomes were isolated according to Hapke & Noll (1976) by zonal centrifugation in 6 mM MgCl₂. The 70s tight-couple peak was pelleted at 40000 rpm for 24 h (45 Ti rotor). The pellets were dissolved in 50 mM sodium cacodylate, pH 7.2, 10 mM MgCl₂, 150 mM KCl, and 3 mM 2-meraptoethanol at a concentration of ~480 A₂₆₀ units/mL. [23]

Example 2: Escherichia coli A19 cells (200g) were disrupted by a French press (10000~15000 psi) in 200 ml of buffer A. After removing the cell debris, the lysate was centrifuged for 45 min at 19600 rpm. The supernatant was laid on 38% sucrose solutions in buffer identical to buffer A except that it contained only 30 mM NH₄Cl and centrifuged for 8 h at 35000 rpm in a BECKMAN 45 Ti rotor at 4 °C. The crude ribosome pellet was then suspended in buffer B and laid on a 20% sucrose solution in buffer B and centrifuged for 4 h at 55000 rpm in a BECKMAN TLA100.3 rotor (crude ribosomal wash). This washing procedure was repeated, after which the salt-washed crude ribosome pellet was resuspended in buffer C. The tight-coupled 70S ribosome was purified from the crude ribosome as described by Shimizu et al. [24]

Example 3: Cell Growth and Preparation of 70S Ribosomes. The wildtype strain *Rhodopseudomonas palustris* CGA009 (a gift from Caroline Harwood, Department of Microbiology, University of Iowa), was grown either aerobically or anaerobically in a glass walled fermentation vessel (Biostat B, B. Braun Biotech, Allentown, PA).⁴⁶ Briefly, aerobic growth conditions, with air injected through the bottom of fermentation vessel, required media supplemented with 10 mM succinate (carbon source) without illumination (to eliminate photosynthesis). Anaerobic growth conditions required 10 mM succinate with the additional requirement of illumination and exclusion of air. All

fermentations were run at 30°C at pH 6.8. Cells were harvested at mid-log growth phase (O.D660 of ~0.8), and washed twice in ice-cold French Press buffer (100 mM ammonium chloride, 50 mM magnesium acetate, 20 mM Tris-HCl (pH 7.5), 1.0 mM DTT, 0.5 mM EDTA). After resuspending cells in the same buffer, a French Pressure cell (Thermo Spectronic, Madison, WI) was used to disrupt cells by applying 16 000 psi 3 times for 1 min. DNase I was added to the resultant suspension to degrade contaminant DNA for subsequent removal. Cellular debris was removed by centrifuging the lysate twice at 30000 × g in a SS-34 Sorval rotor for 30 min at 4°C. The collected supernatant was then quick-frozen with liquid nitrogen and stored at -80°C. [25]

Example 4: The trophozoites of *T. vaginalis* were homogenized in Buffer A containing 6 mM 2-mercaptoethanol with 0.3-mm-/ glass beads by using a microtube mixer (TMW-4836; IWAKI) for 10 min at 4°C. The mixture was centrifuged at 10,000g for 15 min, and the supernatant was saved and removed into a new tube. The pellet was resuspended in Buffer A and centrifuged once more using the same conditions, and the supernatant was removed completely. Ammonium acetate (NH₄Ac) was added to the combined supernatants to a final concentration of 1 M, incubated on ice for 30 min, and centrifuged at 10,000g for 10 min. The supernatant of this high salt-washed ribosome suspension was loaded onto a 10~40% (w/v) linear sucrose density gradient using a high-ionic strength buffer (Buffer D: 1 M NH₄Ac, 15 mM MgCl₂, 2 0mM Tris-HCl, pH 7.6) with 6 mM 2-mercaptoethanol and centrifuged at 40,000 rpm (140,000g) for 3 h in an angle rotor (45Ti; Beckman) at 4°C. The supernatant was fractionated and the absorbance at 260 nm was recorded. The fractions containing small or large ribosomal subunits were collected separately and placed over a 40% (w/v) sucrose cushion in Buffer D. The ribosomes were finally pelleted by centrifugation at 40,000 rpm (99,000g) for 12h at 4°C in an angle rotor (90Ti; Beckman). [26]

2.3 : Motivation

The Ribosome is the universal nano-scale translational machine. But the purification approach of the ribosome is always waste a lot of time, and need ultra-centrifugation many times. It might be break down the natural structure or activity of the ribosome for further applications. The current study tried to find an alternative platform for more rapid purification and basic conformational analysis of the ribosome.



Chapter 3 : Materials and Methods

3.1 : Chemicals

All chemicals, which were of analytical grade or higher, were obtained from Sigma Chemical Co. (St. Louis, MO) or Merck (Darmstadt, Germany).

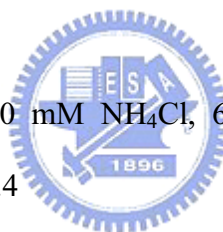
3.1.1 : Buffer solutions for purification of ribosome

Buffer A :

20 mM MgCl₂ 200 mM NH₄Cl, 6 mM 2-mercaptoethanol, 0.1 mM Na₂EDTA, 10 mM Tris-HCl, pH 7.4

Buffer B :

30% sucrose, 10 mM MgCl₂ 500 mM NH₄Cl, 6 mM 2-mercaptoethanol, 0.1 mM Na₂EDTA, 10 mM Tris-HCl, pH 7.4



Buffer C :

10 mM MgCl₂ 50 mM NH₄Cl, 6 mM 2-mercaptoethanol, 0.1 mM Na₂EDTA, 10 mM Tris-HCl, pH 7.4

Phosphate buffer saline (PBS) :

NaCl	8g
Na ₂ HPO ₄	1.44g
KCl	0.2g
KH ₂ PO ₄	0.24g

Then, add deionized water to 1L.

PBS with MgCl₂ :

NaCl	8g
Na ₂ HPO ₄	1.44g

KCl	0.2g
KH ₂ PO ₄	0.24g

Add stock MgCl₂ solution to PBS, final PBS contained 10mM MgCl₂.

PBS with EDTA :

NaCl: 8g

Na₂HPO₄: 1.44g

KCl: 0.2g

KH₂PO₄: 0.24g

Ethylenediaminetetraacetic acid

All buffer were filtered through 0.45 μ m filter before use.

3.1.2 : Solutions for Cryo-Transmission Microscopy

Fixation solution I :

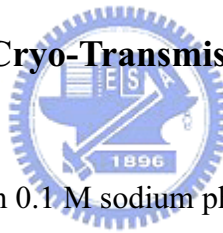
2.5% glutaraldehyde (EM grade) in 0.1 M sodium phosphate buffer , pH 7.4

Fixation solution II :

2% osmium tetroxide

Negative stained solution :

0.5% uranyl acetate



3.2 : Instruments

3.2.1 : Autoclave

Under ordinary circumstances (at standard pressure), liquid water cannot be heated above 100 °C in an open vessel. Further heating results in boiling, but does not raise the temperature of the liquid water. However, when water is heated in a sealed vessel such as an autoclave, it is possible to heat liquid water to a much higher temperature. As the container is heated the pressure rises due to the constant volume of the container. The boiling point of the water is raised because the amount of energy needed to form steam against the higher pressure is increased. This works well on solid objects; when autoclaving hollow objects, however, (hypodermic needles, tools, etc.), it is important to ensure that all of the trapped air inside the hollow compartments is vacuumed out.



Simple autoclaves use a single pulse pre-vacuum, while a modern day autoclave has fractioned pre-vacuum that pulls the air out in several stages to achieve 100% steam penetration in the sterilization process.

Autoclaves are widely used in microbiology, medicine, veterinary science, dentistry and metallurgy.

A medical autoclave is a device that uses steam to sterilize equipment and other objects. This means that all bacteria, viruses, fungi, and spores are inactivated.

Autoclaves are found in many medical settings and other places that need to ensure sterility of an object. They were once more common, but many procedures today

use single-use items rather than sterilized, reusable items. This first happened with hypodermic needles, but today many surgical instruments (such as forceps, needle holders, and scalpel handles) are commonly single-use items rather than reusable.

Because damp heat is used, heat-labile products (such as some plastics) cannot be sterilised this way or they will melt. Some paper or other products that may be damaged by the steam must also be sterilized another way. In stovetop autoclaves, items should always be separated to allow the steam to penetrate the load evenly.

3.2.2 : French pressure cell press

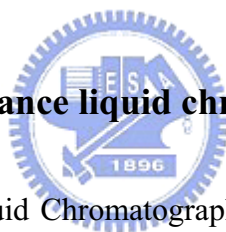
The French pressure cell press, or French press, is an apparatus used in biological experimentation to disrupt the plasma membrane of cells by passing them through a narrow valve under high pressure. The press uses an external hydraulic pump to drive a piston within a larger cylinder that contains the sample. The highly pressurized solution is then squeezed past a needle valve. Once past the valve, the pressure drops to atmospheric pressure and generates shear stress that disrupts the cells. A French press is commonly used to break the resilient plasma membrane and cell walls of bacteria during protein isolation. Some disadvantages of the press include that it is prone to valve clogging, is not well suited to processing of large sample volumes, and is awkward to manipulate and clean due to the weight of the assembly (about 30 lb or 14 kg).

3.2.3 : UV-Visible Spectrophotometer

Ultraviolet/visible absorption spectroscopy, despite the emergence of newer techniques, remains a powerful and important tool. In addition, the instrumentation for UV/Vis spectrophotometer is for the most part relatively inexpensive and widely available. Some instruments are designed specifically to be taken in the field for on-site analyses.

Ultraviolet/visible absorption spectroscopy can be used as a qualitative tool to identify and characterize molecular species (including solvated molecular ions) and as a quantitative tool to assess the quantities of inorganic, organic, and biochemical species present in various samples.

3.2.4 : High-performance liquid chromatography



The High Performance Liquid Chromatography system consisted of one L-2100 pump, L-2200 Autosampler, and L-2450 diode array detector all from Hitachi (Tokyo, Japan). Separations were performed on a BioSep-SEC-S 4000 column (300 X 7.8 mm; phenomenex, Inc.). For large scale purification, a prep column was used (300 X 30 mm). Also see the introduction of instruments of Part I – Page I-32.

3.2.5 : Cryo-Transmission Electron Microscopy

Transmission electron microscopy (TEM) is an imaging technique whereby a beam of electrons is transmitted through a specimen, then an image is formed, magnified and directed to appear either on a fluorescent screen or layer of photographic film, or to be detected by a sensor such as a CCD camera. The first practical transmission electron microscope was built by Albert Prebus and James Hillier at the University of Toronto in 1938 using concepts developed earlier by Max Knoll and Ernst Ruska.



3.3 : Experiments

3.3.1 : Purification of Bacterial Ribosome by

Ultracentrifugation

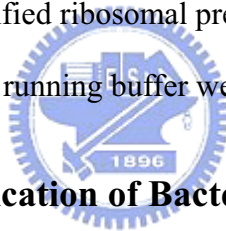
The ultra-centrifugation purification of ribosomes was performed following standard protocol with minor modification [16, 17]. A single colony of *E. coli* XL1-Blue was inoculated into 10 mL LB media at 37 °C for overnight to saturation. The saturated culture was diluted 1/1000 into 1 L LB media and grow with vigorous shaking at 37 °C to mid-log phase which is approximate 1.0 OD at 600nm. The *E. coli* were harvested by centrifugation at 6,500rpm, 4 °C for 30min. The pellet was resuspended in buffer A (20 mM MgCl₂ 200 mM NH₄Cl, 6 mM 2-mercaptoethanol, 0.1 mM Na₂EDTA, 10 mM Tris-HCl, pH 7.4) and disrupted by four passages through French pressure cell (SIM-AMINCO, Taiwan) at 3,000 psi. DNase I was added to a final concentration of 1 µg/mL. The crude extract was centrifuged at 15,000 rpm for 5 minutes to remove cell debris, then at 32,000 rpm for 4 hr at 4 °C in 70Ti rotor (Beckman Coulter). The pellet was resuspended in buffer A and mixed with equal volume of buffer B (30% sucrose, 10 mM MgCl₂ 500 mM NH₄Cl, 6 mM 2-mercaptoethanol, 0.1 mM Na₂EDTA, 10 mM Tris-HCl, pH 7.4). The mixture was centrifuged in a 70Ti rotor at 40,000 rpm for 4 hr at 4 °C. The supernatant was decanted and the clear pellet was resuspended in 1 mL of buffer C (10 mM MgCl₂ 50 mM NH₄Cl, 6 mM 2-mercaptoethanol, 0.1 mM Na₂EDTA, 10 mM Tris-HCl, pH 7.4). Additional spinning at 12,000 rpm for 30 minutes at 4 °C was performed to obtain clear supernatant. The supernatant was dialyzed against buffer C and stored at 4 °C.

3.3.2 : Analysis of Ribosome by HPLC-gel Filtration

All samples were filtered through 0.2 μ m filters before injection. Chromatography buffers were filtered under aspirator vacuum through 0.45 μ m filters. Flow rates were 1 mL/min for analytical column and 5 mL/min for prep column.

We followed the conventional ultra-centrifugal protocol and saved samples at the end of each centrifugation step for HPLC-gel filtration analysis. The crude extract was centrifuged at 15,000 rpm for 5 minutes to remove *E. coli* debris, followed by ultracentrifugation at 32,000 rpm for 1 hr, 40,000 rpm spin for 4 hrs, 12,000 rpm spin for 30 minutes and dialysis against buffer C.

“32000 rpm” denotes partially purified ribosomal prep after 32,000 rpm spin; “40000 rpm” denotes partially purified ribosomal prep after 40,000 rpm spin; and “Final” denotes final dialyzed product. All running buffer were PBS.



3.3.3 : Further Purification of Bacterial Ribosome by HPLC-gel

Filtration

All samples were also filtered through 0.2 μ m filters before injection. Chromatography buffers were filtered under aspirator vacuum through 0.45 μ m filters. Flow rates were 1 mL/min for analytical column and 5 mL/min for prep column.

We followed the conventional ultra-centrifugal protocol and saved samples at the end of each centrifugation step for later HPLC analysis. The crude extract was centrifuged at 15,000 rpm for 5 minutes to remove *E. coli* debris, followed by ultracentrifugation at 32,000 rpm for 1 hr, 40,000 rpm spin for 4 hrs, 12,000 rpm spin for 30 minutes and dialysis against buffer C.

The further purification of ribosomes carried out by HPLC-gel filtration. Partially

purified ribosomes and final dialyzed product were analyzed by HPLC-gel filtration (Figure). All running buffer were PBS with 10 mM MgCl₂.

3.3.4 : Cryo-Transmission Electron Microscopy

Ribosomes were treated with 2.5% glutaraldehyde (EM grade) in 0.1 M sodium phosphate buffer (pH 7.4) and deposited onto 400-mesh copper grids pre-coated with carbon. The grids were fixed with 2% osmium tetroxide and negative-stained with 0.5% uranyl acetate. Images were acquired by JEOL JEM-2010 cryo-transmission electron microscopy (Japan).



Chapter 4 : Results and Discussion

4.1 : Analysis of Ribosome by HPLC-gel filtration

E. coli culture was grown to mid-log phase (Figure 1), harvested, and passed through French press to disrupt the *E. coli*. We followed the conventional ultra-centrifugal protocol and saved samples at the end of each centrifugation step for HPLC-gel filtration analysis. The crude extract was centrifuged at 15,000 rpm for 5 minutes to remove *E. coli* debris, followed by ultracentrifugation at 32,000 rpm for 1 hr, 40,000 rpm spin for 4 hrs, 12,000 rpm spin for 30 minutes and dialysis against buffer C.

Figure 2 shows the each purification process at the end of 32,000 rpm for 1 hr, 40,000 rpm spin for 4hrs, and final dialyzed sample by HPLC-gel filtration analysis. There are three major peaks, the first peak might be the aggregation of ribosome, the second peak might be the 50S subunits, and the third peak thought to be 30S subunits. Other small peaks were smaller molecules. All the samples in Figure 2 used PBS (pH7.4) as the running buffer. Flow rates were 1 mL/min for analytical column and 5 mL/min for prep column.

Figure 3 shows also shows the each purification process at the end of 32,000 rpm for 1 hr, 40,000 rpm spin for 4hrs, and final dialyzed sample by HPLC-gel filtration analysis. There are two major peaks, the first peak might be the aggregation of ribosome, the second peak thought to be the intact 70S ribosome, all the other peaks were smaller molecules. All the samples in Figure 3 used PBS with 10 mM MgCl₂ (pH7.4) as the running buffer. Flow rates were 1 mL/min for analytical column and 5 mL/min for prep column.

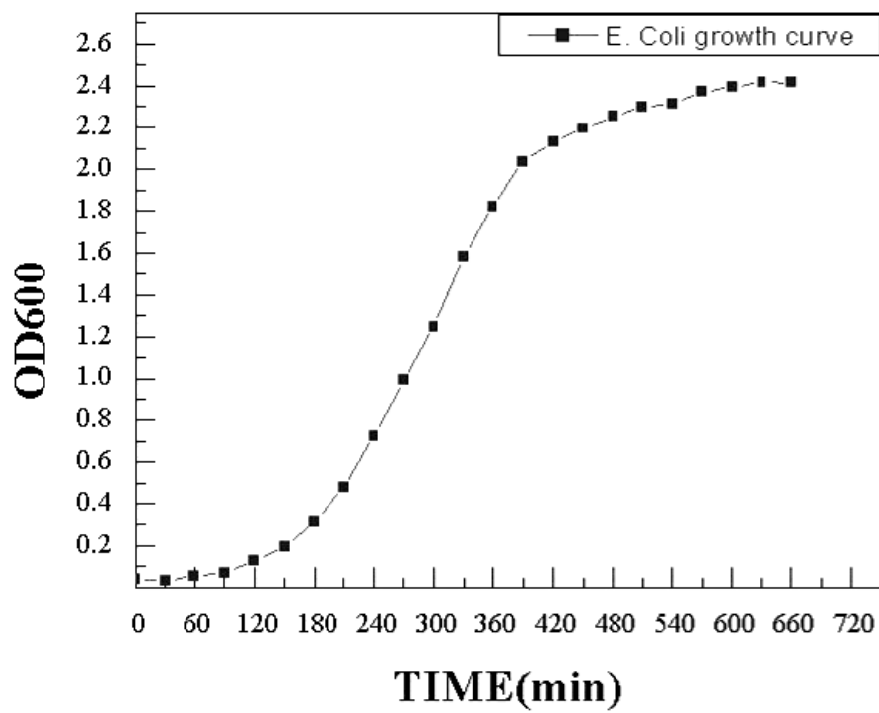


Fig 1: The growth curve of *E. coli* XL1-Blue.

We grew with vigorous shaking at 37 °C to mid-log phase which is approximate 1.0 OD at 600nm to further experiment.

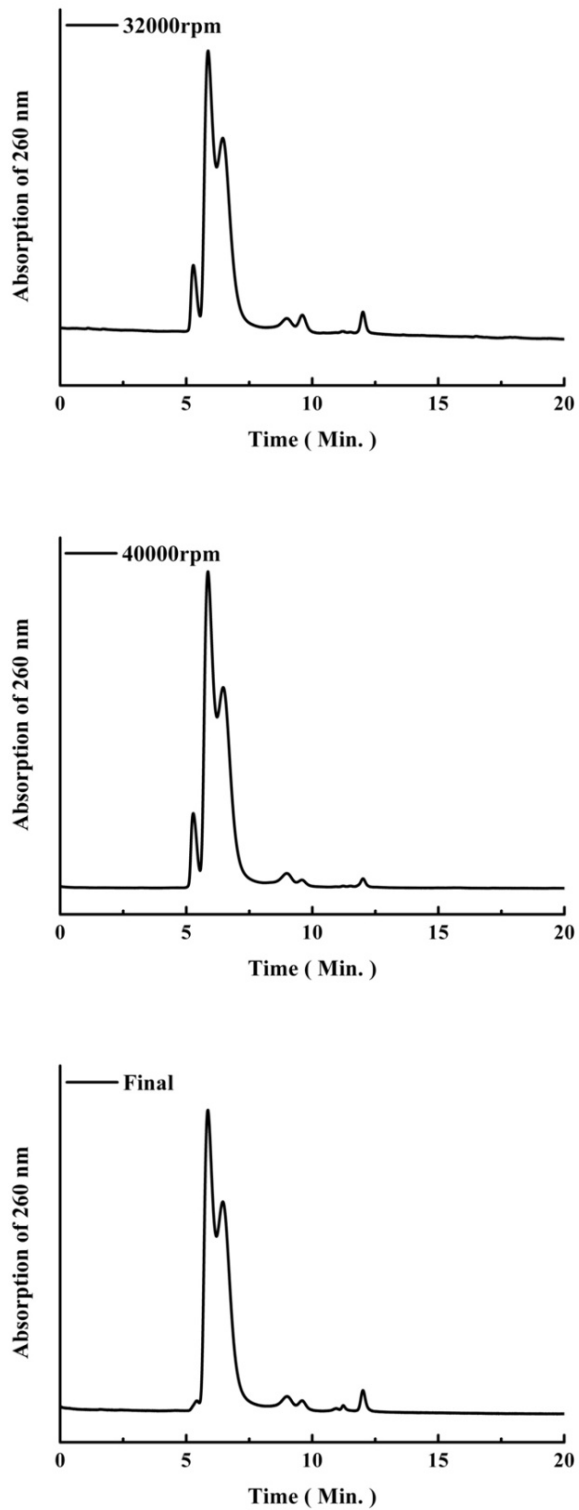


Fig 2: HPLC gel-filtration of each purification process.

- (A) At the end of 32,000 rpm for 1 hr
- (B) At the end of 40,000 rpm for 4 hrs
- (C) At the end of final dialyzed

The running buffer were PBS, pH 7.4.

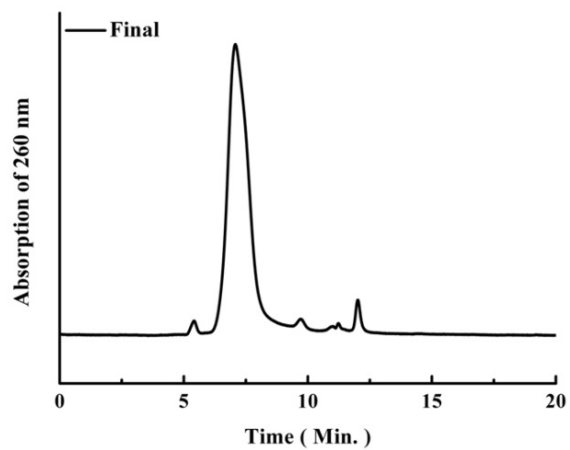
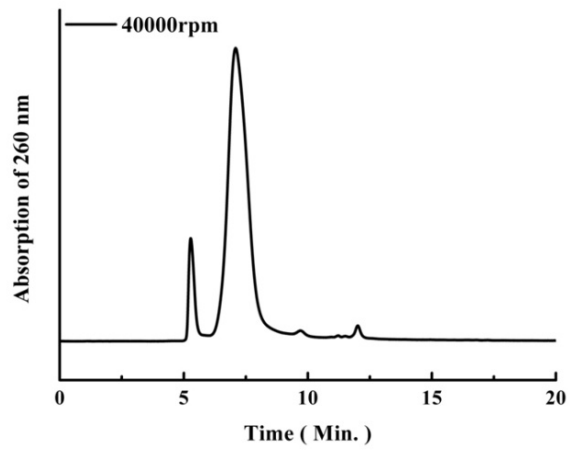
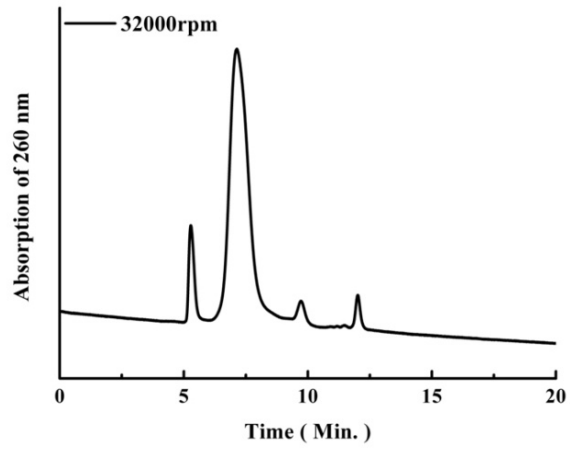


Fig 3: HPLC gel-filtration of each purification process with 10mM MgCl₂.

- (A) At the end of 32,000 rpm for 1 hr
- (B) At the end of 40,000 rpm for 4 hrs
- (C) At the end of final dialyzed

The running buffer were PBS with 10mM MgCl₂, pH 7.4.

4.2 : HPLC further Purification and Analysis for Ribosome

E. coli culture was grown to mid-log phase (Figure 1), harvested, and passed through French press to disrupt the *E. coli*. We followed the conventional ultra-centrifugal protocol and saved samples at the end of each centrifugation step for later HPLC analysis. The crude extract was centrifuged at 15,000 rpm for 5 minutes to remove *E. coli* debris, followed by ultracentrifugation at 32,000 rpm for 1 hr, 40,000 rpm spin for 4 hrs, 12,000 rpm spin for 30 minutes and dialysis against buffer C. Partially purified ribosomes and final dialyzed product were analyzed by HPLC-gel filtration (Figure 4A). A major peak consistently eluted at 7.2 min appeared for all samples. The apparent molecular weight matched 70S ribosome, ca 2,300 kDa. Smaller molecules were abundant in the initial crude extract but gradually disappeared in the final product.

We collected the ribosome fraction using prep column for crude extract and from final dialyzed product. The HPLC-purified ribosomes appeared single peak without impurities in the chromatogram (Figure 4B).

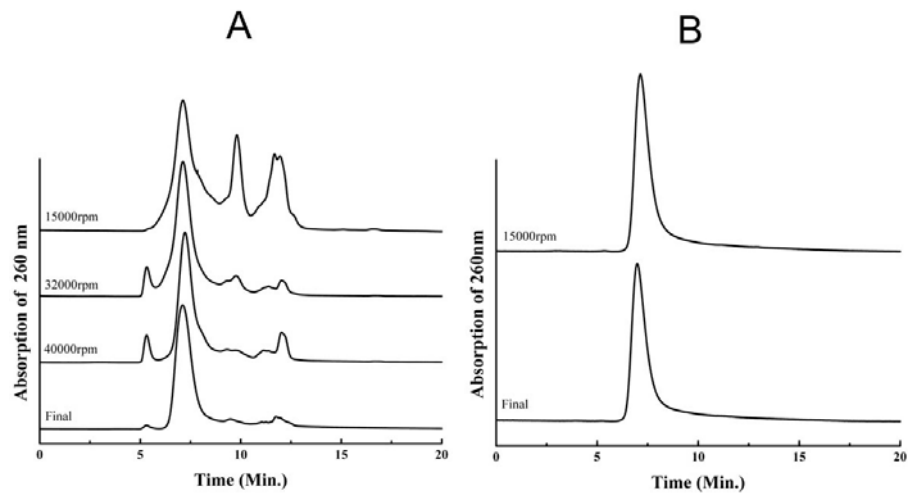


Fig 4: HPLC-gel filtration analysis of prokaryotic ribosomes.

E. coli XL-1 blue is grown to mid-log phase followed by conventional ultracentrifugation procedure. (A) Samples for HPLC injection are taken from crude extract, 32,000 rpm spin, 40,000 rpm spin, and final dialyzed prep. Twenty microliters of 5 mg/mL ribosomes are injected for each run. Ribosomes are eluted as major peak at 7.2 min. (B) Ribosomal fractions are collected from purification of crude extract and final dialyzed prep.

The collected fraction is analyzed by HPLC-gel filtration. “15000 rpm” denotes crude extract; “32000 rpm” denotes partially purified ribosomal prep after 32,000 rpm spin; “40000 rpm” denotes partially purified ribosomal prep after 40,000 rpm spin; and “Final” denotes final dialyzed product. All running buffer were PBS with 10 mM MgCl₂.

Cryo-Electron microscopic image indicated intact 70S ribosome conformation. It can see two unequal subunits clearly. (Figure 5).

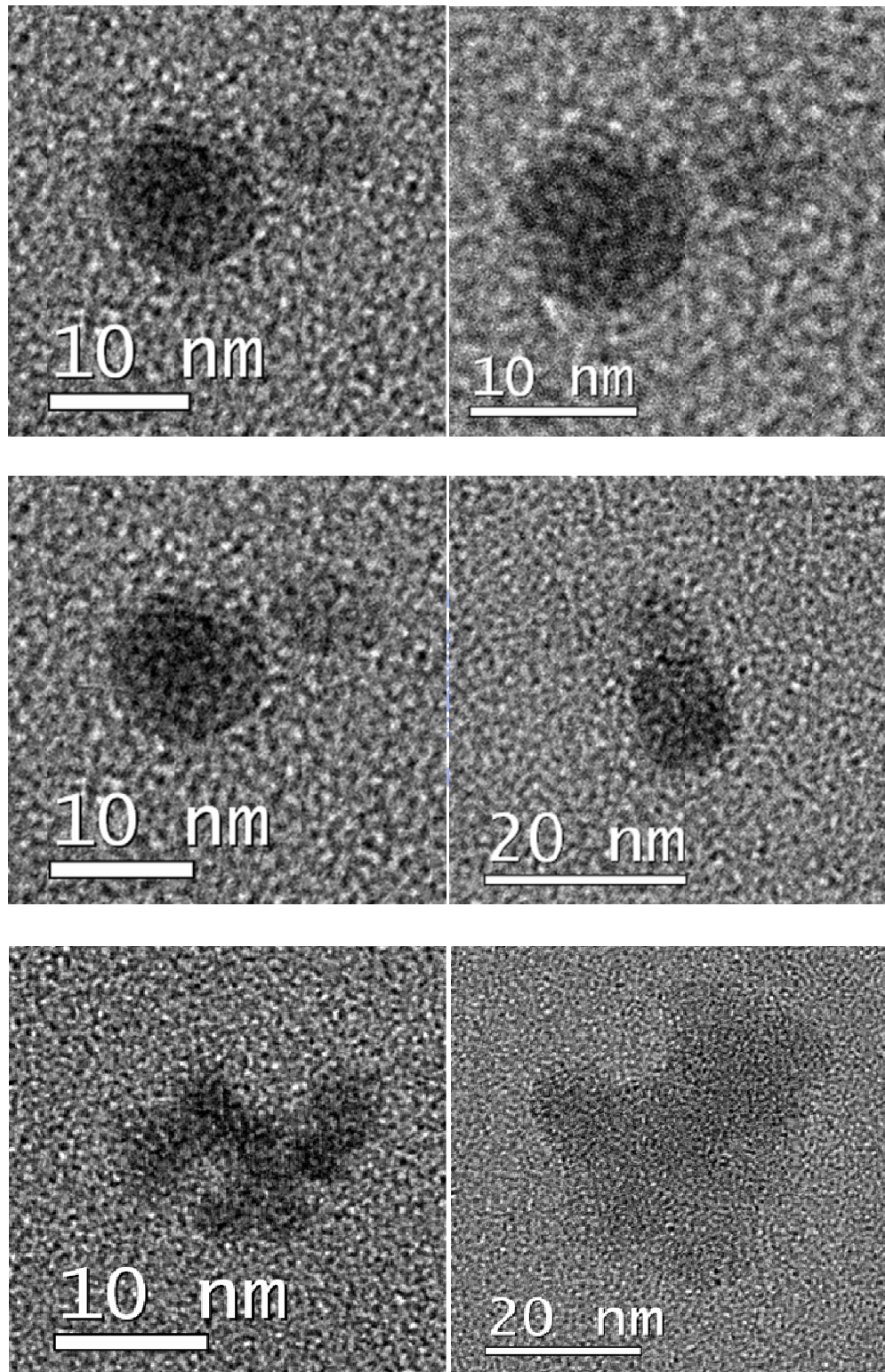


Fig 5: Cryo-Electron microscopic image indicated intact 70S ribosome conformation.

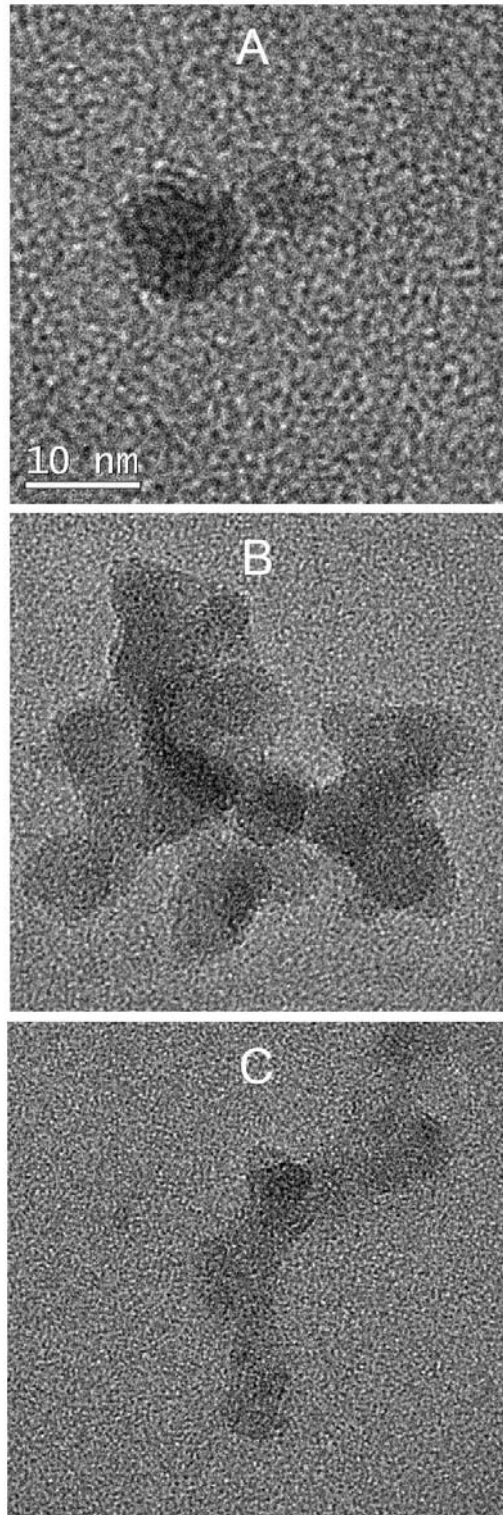


Fig 6: Cryo-EM images of ribosomal fractions collected from HPLC-purification. (A) The purified ribosomes are composed of a 50S subunit of 10 nm in diameter and a 30S subunit of 8 nm in diameter. (B) In the absence of magnesium, HPLC analysis shows aggregation of ribosomes in solution. The 6.2 min fraction appears as aggregates of 50S subunit. (C) The 6.8 min fraction appears to be aggregates of 30S subunit.

HPLC-purified ribosomes in general overwhelmed ultra-centrifugation-purified extracts and reached OD_{260/280} ratio of 2.31 for the best preparation (Figure 7). The OD ratio for HPLC-purification from 15,000 rpm spun crude extract (2.05) was even higher than the final product from ultra-centrifugation protocol (1.92).

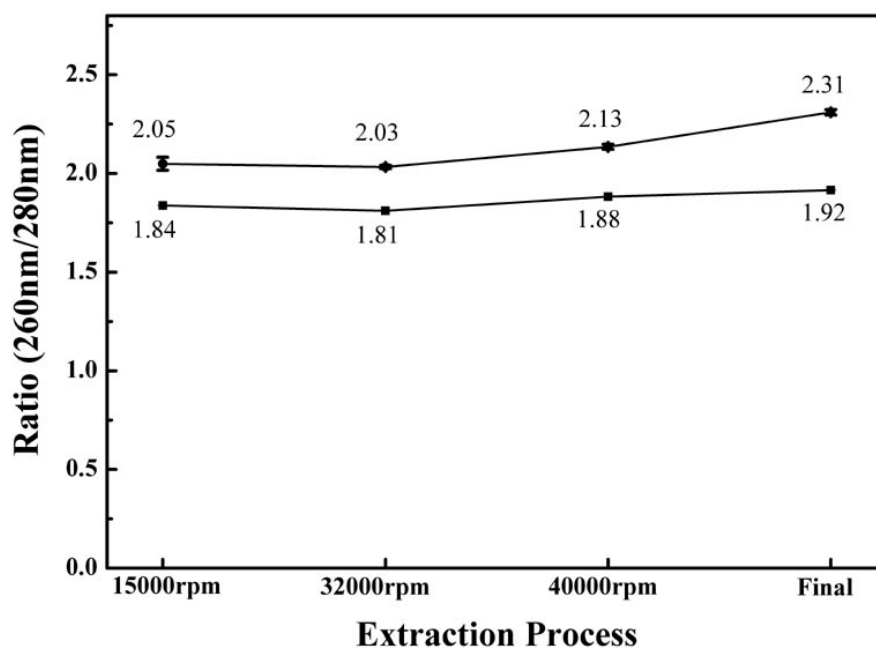


Fig 7: OD_{260/OD280} of HPLC-purified ribosomes compared to ultra-centrifugation-purified prep. Solid squares denotes ultra-centrifugation-purified prep; Solid circles denote HPLC-purified ribosomes.

Thermal stability was measured by incubating ribosomal extract at 37 °C or at 42 °C. HPLC chromatogram showed that HPLC-purified ribosome from crude extract was stable at 37°C but gradually degraded at 42 °C (Figure 8A, 8B). Thermal stability was thus performed at 42 °C for all samples. HPLC-purified dialyzed prep presented best stability, while HPLC-purified crude extract degraded to 30 % in 10 hrs (Figure 8C). Addition of bovine serum albumin (BSA) at 10 mg/mL concentration partially protected the thermal degradation; however, crude extract showed intermediate stability and was more stable than HPLC-purified crude extract. It is likely that residual protease/nuclease activity existed in the HPLC-purified crude extract that degraded the purified ribosomes but partially retarded by the addition of BSA. Addition of PMSF recovered up to 90%

which indicated that protease activity contributed largely to the degradation of ribosomes in the thermal stability test (Figure 8C).

In summary, fast purification of bacterial ribosome could be achieved by a 5 min spin at 15,000 rpm followed by a 10 min run of HPLC-gel filtration, a purification procedure less than 20 min from crude extract.

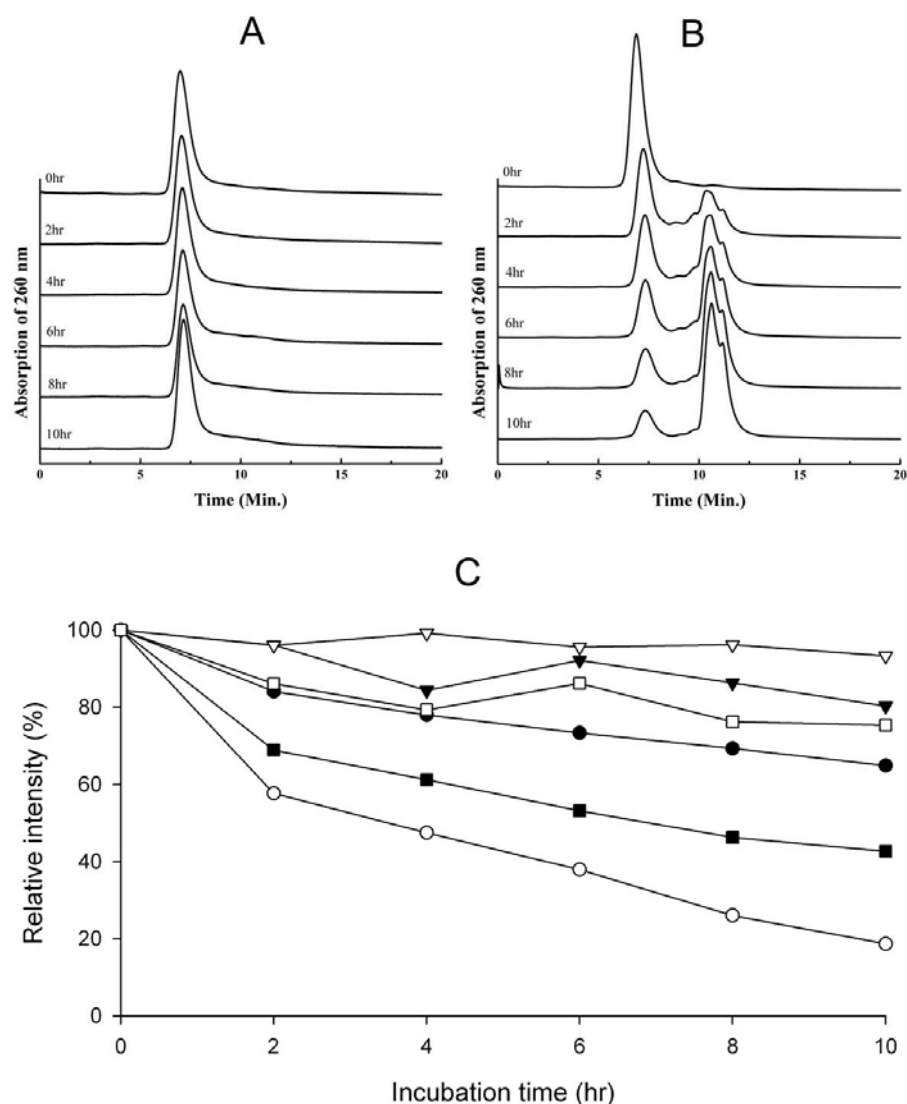


Fig 8: Thermal stability test on HPLC-purified and partially purified ribosomes.

(A) HPLC-purified ribosomes from crude extract are incubated at 37 °C. Analysis is performed on 2 hr interval. (B) HPLC-purified ribosomes from crude extract are incubated at 42 °C. Significant degradation of ribosomal peak is observed. (C) Stability test at 42 °C is performed for HPLC-purified dialyzed product (∇), Purified crude extract with 10mg/ml BSA (▼), Purified crude extract (□), HPLC-purified crude extract (●), and crude extract with 10mg/ml BSA (■), crude extract (○). Initial intensity of ribosomal peak is set at 100%. The data is average of three repeats.

4.3 : The Absence of Magnesium Promoted Aggregation of

Ribosomes

Magnesium ion binds ribosomes and maintains native structure of 70S ribosomes [11-15]. To investigate the structural change in the absence of magnesium, freshly purified ribosomes were analyzed by HPLC at various concentrations of magnesium ions (Figure 9A). We did not observe apparent dissociation of 70S into smaller 50S and 30S subunits. Instead, the 70S peak gradually disappeared and re-appeared as a broader peak eluted at earlier time. The apparent molecular weights for the non-native ribosomes implied that higher order of reorganization might have occurred in the magnesium-free environment. To completely remove magnesium ions, increasing concentration of EDTA was supplemented into the running buffer. In the presence of 5 mM EDTA two peaks appeared at 6.2 and 6.8 min (Figure 9B). To explore the possible conformational reorganization of ribosomes, these two peaks were collected and examined under Cryo-EM (Figure 2B, 2C). In the presence of magnesium, 70 S ribosomes acquired a native conformation; in the absence of magnesium ribosomes appeared aggregates under EM. Judging by the size revealed by EM image, the 6.2 min peak consisted aggregate of 50S subunit while the 6.8 min peak appeared to be aggregate of 30S subunit. The appearance of aggregates revealed molecular sizes and weights much larger than the pore size of exclusion resin. It is likely that the collected peaks contain 50S and 30S subunits respectively. The subunits interacted with each other and presented molecular size larger than 70S but still smaller than the pore size of exclusion resin thus were eluted earlier than 70S ribosome but later than the exclusion peak. During the sample preparation for Cryo-EM, the collected fraction lost water and generated large aggregates. Structural characterization must be performed to verify this

statement.

HPLC has been applied to the analysis and purification for the protein components of ribosomes (ref). Hydrophobic interaction is applied as a final touch in the preparation of ribosomes for crystallography [21]. Affinity HPLC is so far the fastest purification tool [22]. However, both methods lack the ability of analyzing structural variation for the purified ribosomes. Gel-filtration HPLC provides an economic and fast tool to purify ribosomes from crude extract. The ability to resolve structural interaction of ribosomes indicates additional dimension for conformational study.

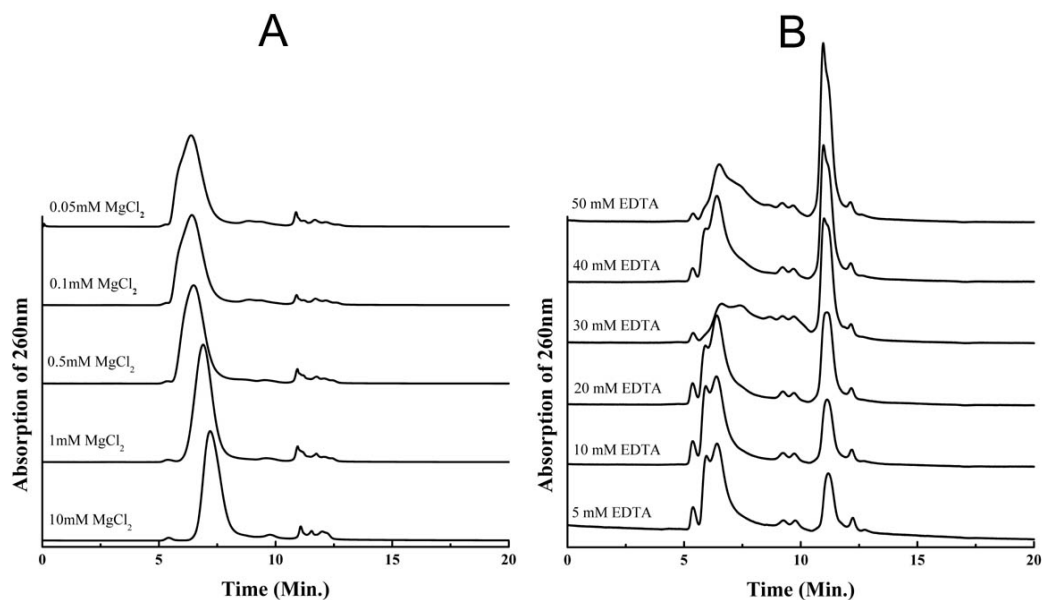


Fig 9: HPLC analysis of purified ribosomes at various concentrations of magnesium ions. (A), and in the presence of EDTA (B). The concentrations of magnesium ions and EDTA are marked on the left of each chromatogram.

Chapter 5 : Conclusion

We applied HPLC-gel filtration system for the analysis and purification of prokaryotic ribosomes. The ribosomes thus purified were optically purer and more stable in solution for storage. The current study provided a fast and convenient procedure alternative for the purification of ribosome. In addition, HPLC was demonstrated as a handy tool to access structural information for ribosomes. There are some problems with our method. Although the ribosome become more purer and more stable, we can not purify great quantity of ribosomes with HPLC-gel-filtration. It is due to the injection volume of gel-filtration column.



Chapter 6 : References

1. V. Ramakrishnan, *Ribosome structure and the mechanism of translation*, Cell, 2002. **108**:p 557.
2. P. Nissen, J. Hansen, N. Ban, P.B. Moore, T.A. Steitz, *The structural basis of ribosome activity in peptide bond synthesis*, Science, 2000. **289**:p 920.
3. B.S. Schuwirth, M.A. Borovinskaya, C.W. Hau, W. Zhang, A. Vila-Sanjurjo, J.M. Holton, J.H. Cate, *Structures of the bacterial ribosome at 3.5 Å resolution*, Science, 2005. **310**:p 827.
4. M.M. Yusupov, G.Z. Yusupova, A. Baucom, K. Lieberman, T.N. Earnest, J.H. Cate, H.F. Noller, *Crystal structure of the ribosome at 5.5 Å resolution*, Science, 2001. **292**:p 883-896.
5. J.H. Cate, M.M. Yusupov, G.Z. Yusupova, T.N. Earnest, H.F. Noller, *X-ray crystal structures of 70S ribosome functional complexes*, Science, 1999. **285**:p 2095.
6. P.B. Moore, *Structural biology. A ribosomal coup: E. coli at last!*, Science, 2005. **310**:p 793.
7. W.M. Clemons, Jr., J.L. May, B.T. Wimberly, J.P. McCutcheon, M.S. Capel, V. Ramakrishnan, *Structure of a bacterial 30S ribosomal subunit at 5.5 Å resolution*, Nature, 1999. **400**:p 833.
8. B.T. Wimberly, D.E. Brodersen, W.M. Clemons, Jr., R.J. Morgan-Warren, A.P. Carter, C. Vornrhein, T. Hartsch, V. Ramakrishnan, *Structure of the 30S ribosomal subunit*, Nature, 2000. **407**:p 327.
9. H. Gao, M.J. Ayub, M.J. Levin, J. Frank, *The structure of the 80S ribosome from Trypanosoma cruzi reveals unique rRNA components*, Proc Natl Acad Sci U S A., 2005. **102**:p 10206. Epub 12005 Jul 10212.

10. K.M. Choi, J.F. Atkins, R.F. Gesteland, R. Brimacombe, *Flexibility of the nascent polypeptide chain within the ribosome--contacts from the peptide N-terminus to a specific region of the 30S subunit*, Eur J Biochem., 1998. **255**:p 409.
11. D.J. Klein, P.B. Moore, T.A. Steitz, *The contribution of metal ions to the structural stability of the large ribosomal subunit*, RNA, 2004. **10**:p 1366.
12. S.H. Allen, K.P. Wong, *The role of magnesium and potassium ions in the molecular mechanism of ribosome assembly: hydrodynamic, conformational, and thermal stability studies of 16 S RNA from Escherichia coli ribosomes*, Arch Biochem Biophys., 1986. **249**:p 137.
13. V. Favaudon, F. Pochon, *Magnesium dependence of the association kinetics of Escherichia coli ribosomal subunits*, Biochemistry, 1976. **15**:p 3903.
14. R.L. Weiss, B.W. Kimes, D.R. Morris, *Cations and ribosome structure. 3. Effects on the 30S and 50S subunits of replacing bound Mg²⁺ by inorganic cations*, Biochemistry, 1973. **12**:p 450.
15. R.L. Weiss, D.R. Morris, *Cations and ribosome structure. I. Effects on the 30S subunit of substituting polyamines for magnesium ion*, Biochemistry, 1973. **12**:p 435.
16. T. Maniatis, E.F. Fritsch, J. Sambrook, *Molecular Cloning*, Cold Spring Harbor Laboratory, Cold Spring Harbor, NY.1982.
17. H.F. Noller, Jr., K. Moldave, *Ribosomes*, in: *Methods in Enzymology*, Academic Press, Inc., San Diego, 1988. **164**:p 428.
18. A.H. Erickson, G. Blobel, *Cell-free translation of messenger RNA in a wheat germ system*, Methods Enzymol., 1983. **96**:p 38.
19. T. Auerbach-Nevo, R. Zarivach, M. Peretz, A. Yonath, *Reproducible growth of well diffracting ribosomal crystals*, Acta Crystallogr D Biol Crystallogr., 2005. **61**:p 713.

20. H. Saruyama, *Isolation of ribosomal subunits from an extremely halophilic archaeobacterium Halobacterium halobium by hydrophobic interaction chromatography*, Anal Biochem., 1986. **159**:p 12.
21. A.I. Nikolaeva, *Isolation of preparative amounts of polyribosomes from normal rabbit and guinea pig spleen*, Biokhimiia, 1976. **41**:p 1753.
22. T. Inada, E. Winstall, S.Z. Tarun, Jr., J.R. Yates, 3rd, D. Schieltz, A.B. Sachs, *One-step affinity purification of the yeast ribosome and its associated proteins and mRNAs*, RNA, 2002. **8**:p 948.
23. Cheow Ling Chiam and Rolf Wagner, *Composition of the Escherichia coli 70s Ribosomal Interface: A Cross- Linking Study*, Biochemistry, 1983. **22**:p 1193.
24. So Umekage, Takuya Ueda, *Spermidine inhibits transient and stable ribosome subunit dissociation*, FEBS Letters, 2006. **580**:p 1222.
25. Michael Brad Strader, Nathan C. VerBerkmoes, David L. Tabb, Heather M. Connelly, John W. Barton, Barry D. Bruce, Dale A. Pelletier, Brian H. Davison, Robert L. Hettich, Frank W. Larimer, and Gregory B. Hurst, *Characterization of the 70S Ribosome from Rhodospseudomonas palustris Using an Integrated “Top-Down” and “Bottom-Up” Mass Spectrometric Approach*, Journal of Proteome Research, 2004. **3**:p 965.
26. Nobuko Arisue, Yasushi Maki, Hideji Yoshida, Akira Wada, Lidya B. Sa' nchez, Miklo's Muller,³ Tetsuo Hashimoto, *Comparative Analysis of the Ribosomal Components of the Hydrogenosome-Containing Protist, Trichomonas vaginalis*, J Mol Evol, 2004. **59**:p. 59.